

ABSTRACT

Detailed Paleoclimatic Records from Late Pennsylvanian Polygenetic Paleosols: North-Central Texas, USA

Amos Culbertson, M.S.

Committee Chairperson: Steven G. Driese, Ph.D.

Two Canyon Group (late-Pennsylvanian, Missourian) multistory, polygenetic paleosol intervals in north-central Texas, USA record complex paleoclimatic and paleohydrologic histories. Both paleosol intervals show evidence for initial development under well-drained conditions (illuviated clay, pedogenic calcite nodules, high-chroma matrix colors) and are overprinted by features that indicate poorer drained conditions (gley matrix colors, pedogenic siderite), however overprinting occurred through rapid transgression in one paleosol and gradual sea-level rise in the other. Reconstructed physical and wet chemical soil properties indicate these paleosols were finely textured, fertile, and void of salinity problems. Paleatmospheric pCO₂ estimates from the $\delta^{13}\text{C}$ values of pedogenic calcite nodules indicate values near pre-industrial levels (360ppmV), which are in agreement with previously published proxy and modeling results. This study shows that despite multiple episodes of overprinting, a detailed paleoclimatic and paleohydrologic history can be reconstructed from paleosols using careful macro and micromorphological observations.

Detailed Paleoclimatic Records from Late Pennsylvanian
Polygenic Paleosols: North-Central Texas, USA

by

Amos Culbertson, B.S.

A Thesis

Approved by the Department of Geology

Steven G. Driese, Ph.D., Chairperson

Submitted to the Graduate Faculty of
Baylor University in Partial Fulfillment of the
Requirements for the Degree
of
Master of Science

Approved by the Thesis Committee

Steven G. Driese, Ph.D., Chairperson

Steven I. Dworkin, Ph.D.

Stacy C. Atchley, Ph.D.

Joseph D. White, Ph.D.

Accepted by the Graduate School
August 2013

J. Larry Lyon, Ph.D., Dean

Copyright © 2013 by Amos Culbertson

All rights reserved

TABLE OF CONTENTS

List of Figures	v
ACKNOWLEDGMENTS	vi
CHAPTER ONE	
Introduction	
<i>Significance of study</i>	1
CHAPTER TWO	2
Manuscript One	2
<i>Abstract</i>	2
<i>Introduction</i>	3
<i>Location and Methods</i>	4
<i>Stratigraphy and Depositional Setting</i>	6
<i>Outcrop Descriptions</i>	7
<i>Micromorphology</i>	8
<i>Geochemistry, Clay Mineralogy, and Organic Carbon</i>	10
<i>Paleoatmospheric PCO₂</i>	13
<i>Discussion and Interpretations</i>	13
<i>Conclusions</i>	17
CHAPTER THREE	33
Conclusion	33
APPENDICES	34
Appendix A – Bulk Geochemical Data	34
Appendix B – Stable Isotopic Composition of Pedogenic Calcite	45
Appendix C – Stable Isotopic Composition of Soil Organic Carbon	47
REFERENCES	51

LIST OF FIGURES

Figure 1	Location map of the Lake Brownwood Spillway study area	20
Figure 2	Paleogeographic map of the study area	21
Figure 3	Stratigraphic section of the Lake Brownwood Spillway	22
Figure 4	Outcrop sections of the Lake Brownwood Spillway paleosol intervals	23-24
Figure 5	Thin section photomicrographs of paleosols	25
Figure 6	CALMAG paleoprecipitation estimates from paleosols	26
Figure 7	Reconstructed physical and chemical properties of the Lake Brownwood Spillway paleosols	27
Figure 8	X-ray diffraction patterns	28
Figure 9	Weight percent total carbon values	29
Figure 10	Paleoatmospheric pCO ₂ estimates	29
Figure 11	Proposed paleoprecipitation and paleohydrology model for the lower paleosol interval	30
Figure 12	Proposed paleoprecipitation and paleohydrology model for the lower paleosol interval	31

ACKNOWLEDGMENTS

I would like to acknowledge my advisor Dr. Steven Driese for his encouragement and assistance on almost every level of this project, as well as my thesis committee members for their contribution. I would like to thank the Geological Society of America, and the National Science Foundation for their financial assistance with this project. Lastly I would like to thank my friends and family for their support through this period of my education.

CHAPTER ONE

Introduction

The late Pennsylvanian is a good ancient analog for current global conditions because it is our only record of a transition from a glaciated world to a non-glaciated world since the rise of plants, and it is the last time in earth's history that paleoatmospheric pCO₂ levels were comparable to modern day levels. This study takes advantage of a unique opportunity to do a paleoclimate study on a time period that could lead to a better understanding of the future of climate change. The paleosols at the Lake Brownwood Spillway provide window into the climate and ecosystem that existed in central Texas prior to the end of the Late Paleozoic Ice Age and provides an opportunity to apply some new proxies to Paleozoic paleosols that are diagenetically immature.

This thesis was formatted for submission to the Journal of Sedimentary Research and was solely authored by Amos Vincent Culbertson.

CHAPTER TWO

Detailed Paleoclimatic Records from Late Pennsylvanian Polygenetic Paleosols: North-Central Texas, USA

Abstract. Two Canyon Group (late-Pennsylvanian, Missourian) multistory, polygenetic paleosol intervals in north-central Texas, USA record complex paleoclimatic and paleohydrologic histories. Both paleosol intervals show evidence for initial development under well-drained conditions (illuviated clay, pedogenic calcite nodules, high-chroma matrix colors) and are overprinted by features that indicate poorer drained conditions (gley matrix colors, pedogenic siderite), however, overprinting occurred through different processes. The lower paleosol interval (LPI) remained better-drained until the upper horizon was saturated via top-down wetting following inundation during transgression, presumably as the result of relatively rapid sea-level rise. The upper paleosol interval (UPI) was initially better-drained, but drainage became progressively poorer during the time of its formation likely due to gradual regional water table rise associated with a slower rate of sea-level rise during transgression. Paleoprecipitation estimates using the CALMAG proxy for vertic (Vertisol-like) paleosols averaged 1300 mm/yr for both intervals, with notable excursions to drier conditions (700 mm/yr) in each. The degree of development of vertic features in the paleosols was used to estimate the seasonality of paleoprecipitation, which increased from weakly to strongly seasonal during the development of the LPI, but remained strongly seasonal throughout the development of the UPI. Reconstructed physical and wet chemical soil properties indicate these paleosols were finely textured, fertile, and void of salinity problems. Paleoatmospheric pCO₂

estimates from the $\delta^{13}\text{C}$ values of pedogenic calcite nodules indicate values near pre-industrial levels (360ppmV), which are in agreement with previously published proxy and modeling results. This study shows that despite multiple episodes of overprinting, a detailed paleoclimatic and paleohydrologic history can be reconstructed from paleosols using careful macro and micromorphological observations.

INTRODUCTION

The late Pennsylvanian marks the beginning of the demise of the late Paleozoic ice age, and represents the only transition of our world from icehouse to greenhouse conditions since plants colonized the earth (Tabor and Montañez 2002; Tabor and Poulsen 2008; Montañez et al. 2007). Geochemical proxy and computer modeling results indicate that paleoatmospheric pCO_2 levels were comparable to modern atmospheric levels (Montañez et al. 2007; Berner 2006; Royer et al. 2001; Beerling 2002). For these reasons the late Paleozoic ice age is an excellent ancient analog for current global conditions (Raymond and Metz 2004). Canyon Group paleosols in north-central Texas, U.S.A. provide a unique opportunity to conduct a detailed study of low-latitude paleoclimatic conditions on western Pangea during the late Pennsylvanian.

In this paper we use a combination of field, micromorphological, and geochemical techniques to demonstrate that: (1) these paleosols exhibit features that record a complex history of changes in paleohydrology, paleoprecipitation, and paleoprecipitation seasonality related to regional and local climate variability. Nevertheless, a detailed history of soil genesis can be interpreted in spite of the fact that there has been overprinting of multiple paleosols stacked on top of one another; (2) reconstructed physical and colloidal properties that cannot be measured in rock paleosols,

namely percent total clay, percent fine clay, pH, bulk density, COLE (coefficient of linear extensibility), base saturation, EC (electrical conductivity), and ESP (exchangeable sodium percentage) compare well with directly measured physical and chemical data from a modern analog Vertisol soil series from the Texas Gulf Coast (Driese and Ober 2005; Nordt and Driese 2010b). Results indicate the paleosols were finely textured, fertile, devoid of sodicity or salinity problems, and would have readily supported plant growth; and (3) paleoatmospheric pCO₂ estimates from soil-formed calcite nodules average 360 ppmV, which is in agreement with previously published proxy and computer modeling results for the late Pennsylvanian, and are appropriate values for icehouse conditions (Cerling 1991; Mora et al. 1996; Berner 2006; Royer et al. 2001; Montañez et al. 2007).

LOCATION AND METHODS

Two late Pennsylvanian (Missourian) Canyon Group paleosol intervals, measuring 3.6 and 4.4 m in thickness, respectively, were examined at the Lake Brownwood Spillway near the city of Brownwood, Texas (Fig. 1). The Lake Brownwood Spillway has experienced episodes of accelerated erosion due to intermittent flooding, which makes it exceptional for paleosol investigations, especially because outcrops of mudrocks in the area are scarce.

Paleosol outcrops were described via the methods of Retallack (1988, 2001). Paleosol colors were described from moist samples in the field using Munsell soil color charts. Samples were collected at 20 cm intervals for bulk geochemical and density analysis. Powdered samples were commercially analyzed for major minor and trace elements using a combination of XRF and ICP-MS analysis techniques. Multiple samples

from both paleosol intervals were analyzed for clay mineralogy using oriented aggregate mounts and the appropriate heat and salt solution treatments. Oriented samples were collected for micromorphological analysis, and thin sections were described following the methods of Brewer (1976) and Fitzpatrick (1993). Cathodoluminescence (CL) investigations of thin sections containing pedogenic calcite utilized a Relion cold-cathode luminescence microscope operated at 6-10 kV and 50-150 μ A to examine calcite recrystallization fabrics at the CL Microscopy Laboratory at Baylor University.

Bulk paleosols samples were powdered, weighed, and treated with 10% HCl ten times before being analyzed for total organic carbon (TOC). Organic matter in the samples was combusted in a Costech elemental analyzer and the resulting CO₂ was analyzed by continuous flow in a Thermo Scientific Delta-V gas-source mass spectrometer at Baylor University's Stable Isotope Laboratory (standard error is \leq 0.04‰). Values are reported here in per mil (‰) standard delta notation, with reference to the Pee Dee Belemnite (PDB) standard, using the following equation:

$$\delta^{13}\text{C}_{\text{om}} (\text{‰}) = \left\{ \left[\frac{{}^{13}\text{C}_{\text{sample}}/{}^{12}\text{C}_{\text{sample}}}{{}^{13}\text{C}_{\text{VPDB}}/{}^{12}\text{C}_{\text{VPDB}}} \right] - 1 \right\} \times 1000$$

Pedogenic calcite samples were collected from all Bk horizons, microdrilled using dental drill bits from cut nodules, and $\delta^{13}\text{C}$ and $\delta^{18}\text{O}$ values were also determined at Baylor University. Samples were loaded into a Thermo Scientific Gasbench II before being reacted with 100% phosphoric acid. The CO₂ gas evolved was then introduced into a continuous-flow Thermo Scientific Delta-V mass spectrometer at Baylor University. Repeat isotope analysis of an in-house standard gives an analytical uncertainty of $\pm 0.16\text{‰}$ for carbon and $\pm 0.07\text{‰}$ for oxygen, reported relative to the VPDB standard using standard delta per-mil (‰) notation.

A modern analog League series Vertisol from east Texas, originally sampled by Driese et al. (2005) as part of their Vertisol climosequence study, was used for comparisons with physical and colloidal chemistry of late Pennsylvanian paleosols (estimated using pedotransfer functions of Nordt and Driese, 2010b) because the League is morphologically similar, is forming within a precipitation regime similar to that inferred for the paleosols based on the CALMAG paleoprecipitation proxy (Nordt and Driese 2010a).

STRATIGRAPHY AND DEPOSITIONAL SETTING

The study area in central Texas was located on the western coast of equatorial Pangea on the eastern margin of the Midland Basin during the late Pennsylvanian (Fig. 2; Brown et al. 1990; Scotese 2003; Blakey 2003, 2010). During this time period the study site was located at approximately 5° south latitude, but drifted northward through the end of the Pennsylvanian and Permian (Scotese 2003; Blakey 2010). Climate modeling results indicate the study site was located in a humid, monsoonal climate region that straddled the equator, but many climatic controls were operating at multiple time scales resulting in a complex and dynamic paleoclimate regime (Tabor and Poulsen 2008).

The section is comprised of interbedded mudrock paleosols, marine carbonates, and marine shales deposited on the broad, low-angle Eastern Shelf of the Midland Basin as it subsided throughout the late Paleozoic (Figs. 2, 3; Brown et al. 1990; Yang 1996; Yang et al. 1998). Glacio-eustatic sea-level changes were a major control on accommodation during this time period, but mixed carbonate-siliciclastic lithologies in the section are attributed to regional topographic controls on depocenter and bypass zones, and climatic controls on siliciclastic supply (Yang 1996; Yang et al. 1998; Yancey

and Cleaves 1990; Yancey 1991; Brown 1990). Siliciclastic sediments were derived from the Ouachita fold belt to the east and deposited as part of a muddy, fluvial-deltaic system that prograded across the Eastern Shelf during the late Pennsylvanian and interfingered with carbonate deposits on the broad Eastern Shelf (Brown 1990; Yancey and Cleaves 1990).

OUTCROP DESCRIPTIONS

Both the upper (UPI) and lower (LPI) paleosol intervals each contain more than one paleosol profile welded on top of one another, and exhibit considerable lateral variability along outcrop, which makes subdividing paleosol units into horizons somewhat complicated. However, both paleosol intervals have oxidized Bk or Bt horizons with high-chroma colors, clay films on ped faces, and/or pedogenic calcite nodules overlain by Bssg horizons with low-chroma (gley) colors, and wedge peds created by pedogenic slickensides (Figs. 4A, B). Both paleosol intervals display well-developed gilgai micro-topography similar to that observed in modern Vertisols, along with the slickensided (ss) horizons (Figs. 4A, B; Driese and Ober 2005; Mintz et al. 2011).

Lower Paleosol Interval (LPI)

The lower part of the LPI is dominated by high-chroma Bt and Bk horizons with stage 2 pedogenic calcite nodules ≤ 2 cm in diameter (Gile et al. 1966), clay films on ped faces, FeMn concentrations, and gley-colored root traces in an oxidized matrix (Fig. 4B). At 1.5 m depth there is a 15 cm thick, prominent, gley colored, fine-grained sandstone with sparse root traces that pinches out between laterally adjacent outcrops 20 m away

(Fig. 4B). The sandstone is overlain by a high-chroma, Bssk horizon with well-developed slickensides, gleyed root traces, stage 2 pedogenic calcite nodules up to 15 cm in diameter, and pedogenic calcite rhizocretions consisting of stacked calcite nodules up to 5 cm in diameter (Fig. 4B; Gile et al. 1966). The uppermost horizon is a gleyed and slickensided Bssg horizon with *Glossifungites* ichnofacies firm ground burrows penetrating down from the overlying limestone to ≤ 5 cm depth (Fig. 4B).

Upper Paleosol Interval (UPI)

The UPI contains Bt and Bk horizons with stage 2 pedogenic calcite accumulations, evidence of clay illuviation, and FeMn concentrations similar to that observed in the LPI, but unlike the UPI there are well-developed slickensides throughout, and the overall matrix is dominated by gley colors (Fig. 4A; 5G). As was the case for the LPI, the UPI also has a sandstone bed at ~ 1.5 m depth that shows minimal alteration by pedogenic process, and has preserved relict bedding structures (Fig. 4A). The upper part of the UPI is gleyed and slickensided with black, coalified root traces, and pedogenic siderite spherules (Figs. 4A, 5F).

MICROMORPHOLOGY

Matrix B-Fabrics

Birefringent fabric (b-fabric) develops in clayey soils as a result of shrink-swell processes related to wet/dry cycles, which causes clay particles to align parallel to each other and appear birefringent under cross-polarized light (Fitzpatrick 1993). Parallel-striated b-fabric (one direction of preferred clay orientation) is common in the upper horizons of the LPI and throughout UPI, but not in the fine-grained sandstone horizons

(Fig. 5A). Granostriated b-fabric, (b-fabric developed around grains, peds, or hard nodules where stress due to clay expansion is high) is present in both paleosol intervals surrounding pedogenic calcite nodules (Figs. 5B, C, H).

Pedogenic Calcite Nodules

The pedogenic calcite nodules in the Lake Brownwood Spillway paleosols are chiefly micrite or microspar with septarian cracks that radiate from the center of the nodule and are filled with one (or more) sparry calcite fabrics that luminesce bright yellow to orange when examined using cathodoluminescence (CL) microscopy (Figs. 5B, H). Some of the nodules contain calcite fragments inherited from older paleosols or from limestone parent material (Fig. 5 H; cf. Michel et al. 2013). Pedogenic calcite nodules from the Bkss horizon of the LPI have FeMn corrosion rims that penetrate 100 to 300 μm into the margins of the nodule (Fig. 5C).

Illuviated Clay

Illuviated clay forms when soil waters translocate clay downward through the profile and the clay particles plate out on pore walls as a result of electrostatic forces that exist between the positive and negatively charged surfaces of clays (Fitzpatrick, 1993). Illuviated clay appears as gold-colored, highly birefringent accumulations that fill pores and cracks (Figs. 5D and E), or coats ped faces (Fig. 4B). These pedofeatures co-occur with pedogenic calcite nodules in most places and are identified in the LPI from 1.8 to 2.9 m depth, and in the UPI from 1.6 to the contact with the underlying limestone (Figs. 4A, B). Reworked clay skins, pedogenic calcite nodules, and peds are present below the sandy BCg horizons in both paleosol intervals (Figs. 5D and G), however in the Btkb

horizon of the LPI there is evidence of clay illuviation that is both pre- and post-reworking of the soil material (Fig. 5D).

Pedogenic Siderite

Microspherules of soil-formed siderite (sphaerosiderite, *sensu* Ludvigson et al., 1998 and Driese et al., 2010) occur as clusters of poorly crystalline reddish crystals that appear to pseudomorph paleo root channels, and are commonly associated with organic material (Fig. 5F). The siderite microspherules are uniform in size and less than 100 μm in diameter (Fig. 5F). CL examination of the pedogenic siderite revealed some minor admixtures of calcite with the siderite.

GEOCHEMISTRY, CLAY MINERALOGY, AND ORGANIC CARBON

Paleoprecipitation

The CALMAG paleoprecipitation proxy relates the bulk geochemistry of a paleosol to the degree of chemical weathering that the soil has experienced, which is related to mean annual precipitation (Nordt and Driese 2010a). CALMAG was chosen for this study (over Sheldon et al.'s 2002 "universal" CIA-K paleoprecipitation proxy) because it was developed using only the B-horizons of modern Vertisols, and almost all of the B-horizons in the Lake Brownwood Spillway paleosols exhibit vertic features (note: horizons without vertic features were excluded from the calculations). CALMAG is defined as $\{Al_2O_3/(Al_2O_3+CaO+MgO)\}$ with an r^2 value of 0.90 for the relationship between the weathering index and MAP, and a root mean square error of ± 108 mm/yr precipitation (Nordt and Driese 2010a). The derived CALMAG values for the Lake Brownwood Paleosols were found to estimate paleoprecipitation of 1200-1300 mm/yr,

with notable deviations to drier conditions in the Bsskb horizon of the UPI (680 mm/yr), and the Bssk horizon of the LPI (720 mm/yr; Fig. 6).

Physical And Chemical Soil Properties

In order to increase the understanding of the soil conditions that existed in these paleosols and which made it possible for them to support late Pennsylvanian ecosystems, bulk oxide geochemical data were used to estimate the original physical and chemical properties of the paleosols via the pedotransfer functions developed by Nordt and Driese (Table 1; 2010b). The results were compared with measured physical and colloidal properties from the League series soil of east Texas (Fig. 7). The League series was chosen as a modern analog because it is a Vertisol that is forming under a precipitation regime similar to that estimated for the Lake Brownwood Spillway paleosols (strongly seasonal, MAP circa 1380 mm/yr), as well as forming from calcareous, clay-rich alluvial deposits likely similar to what the Lake Brownwood Spillway paleosols formed from (Nordt and Driese 2010b).

The Lake Brownwood Spillway paleosols have total clay, fine clay, and COLE values similar to the League series Vertisol, which are consistent with macro- and micromorphological observations. This suggests that these were finely textured soils with a high propensity for shrink-swell processes (Figs. 4A, B, 5A, B, H, 8A, B, C). The reconstructed bulk density values for the Lake Brownwood Spillway paleosols are lower than those of the League series (Fig. 7D), but they have higher estimated total clay and fine clay percentages (Fig. 7A, B), which accounts for the discrepancy of densities between the paleosols and the modern analog. Reconstructed soil pH values for the paleosols are near neutral like those measured in the League series, but increase in the

horizons with greater pedogenic calcite concentrations because of the acid neutralizing capabilities of calcite. Reconstructed Fe_d (Fe extractable from Fe oxides and oxyhydroxides) values are marginally higher than those measured in the modern soil but still below 5% (Fig. 7F). Reconstructed Fe_d values appear to be higher in the high-chroma red paleosol horizons than in the gleyed horizons (Figs. 4A, B, 8F). Reconstructed base saturation values compare well with those measured in the League series and are above 80% in both intervals, but increase to 100% in the horizons with the greatest pedogenic calcite accumulations (Figs. 4A, B, 7G). Reconstructed electrical conductivity and exchangeable sodium percentage values are in reasonable agreement with those measured in the League series soil, and are within the range expected for normal soil conditions (Figs. 8H, I; Brady and Weil 2002).

Clay Mineralogy

The matrix of the paleosols is dominated by kaolinite and illite with small amounts of vermiculite (Moore and Reynolds 1997; Fig. 8). All the samples analyzed had the same clay mineralogical composition, but with some variability in the relative proportion of clay types (Fig. 8).

Organic Carbon

Depth distributions of total organic carbon (TOC) values measured in the Lake Brownwood Spillway paleosols resemble those measured in modern soils, with the highest values in the upper horizons and a decrease in TOC content with depth (Fig. 9; Retallack 2001; Huang et al. 1996). The TOC values are not unlike those measured in modern Vertisols (Brady and Weil 2002), and are higher than those measured in clay rich

paleosols from the Permian-Triassic boundary (<0.3% Krull and Retallack 2000). High amounts of residual soil organic carbon indicate that these soils would not have been limited by nitrogen or sulfur availability.

PALEOATMOSPHERIC PCO₂

Paleoatmospheric pCO₂ estimates were generated using Cerling's (1991,1999) paleosol barometer and twelve $\delta^{13}\text{C}$ values from different pedogenic calcite nodules in both paleosol intervals (Fig. 10). Estimates range from 200 to 720 ppmV based on a 1.33‰ variation in the $\delta^{13}\text{C}$ values, and the range of S(z) values used in the calculations (Fig. 10). S(z) values of 1000 to 3000 ppmV were chosen based on recent work done to better constrain S(z) when applying the paleobarometer proxy to paleo-Vertisols (Fig. 10; Breecker et al. 2013; Montañez 2013; Mintz et al. 2011). A purely C3 plant soil-respired CO₂ $\delta^{13}\text{C}$ value of -23‰ was used based on stable isotopic analysis of organic carbon in the paleosols, which is in agreement with modeled values for late Pennsylvanian vegetation based on the $\delta^{13}\text{C}$ of temporally equivalent marine carbonates (Mora et al. 1996; Veizer et al. 1999). An atmospheric CO₂ $\delta^{13}\text{C}$ value of -3.5‰ was modeled from the $\delta^{13}\text{C}$ values for the seawater curve of Veizer et al. (1999).

DISCUSSION AND INTERPRETATIONS

Soil Genesis and Paleoprecipitation

Lower Paleosol Interval (LPI).—The LPI exhibits a number of pedofeatures indicating that initial drainage conditions were good including high-chroma, oxidized soil matrix colors, illuviated clay accumulations, pedogenic calcite nodules, and pressure faces on peds (Figs. 4B, 5D). Paleoprecipitation estimates increase slightly from ~1300 to

1400 mm/yr between the 4.3 m and 1.7 m depth, possibly suggesting that the climate became wetter while the lowermost paleosol profile developed (Fig. 6, 11). Above this unit, the interval is divided by a gley colored, laterally discontinuous, fine-grained sandstone that was probably deposited as a crevasse splay event during a period of paleo-channel instability (Fig. 4B). There is evidence of reworked peds and clay skins in a sandy matrix overprinted by illuviated clay features indicating low (at least seasonally low) paleo-water table levels before and after the event (Fig. 5, 11). This event was followed by a period of prolonged landscape stabilization and drier conditions as indicated by the large (15 cm in diameter) pedogenic calcite nodules and rhizcretions, and CALMAG paleoprecipitation estimates of as low as 680 mm/yr (Figs. 4B, 6). The Bssg horizon at the top of the interval points a wetter and more seasonal precipitation regime as indicated by well-developed slickensides, birefringent matrix fabrics (b-fabric), pedogenic calcite nodules with FeMn corrosion rims, and paleoprecipitation estimates as high as 1400 mm/yr (Figs. 4A, 5A, C, 6, 11). The pervasive gleying of the upper horizon could be due to a long term rise in the water table associated with transgression, or top-down overprinting via marine hydromorphism (e.g. Driese and Ober 2005). The latter explanation is favored because the gleying exists only in the upper 80 cm or less of the profile, and the contact between the gleyed and oxidized horizons is irregular and undulatory, which is suggestive of top-down wetting from a fluid front moving downward through the profile rather than prolonged saturation due to high water-table levels. Also this profile lacks pedogenic siderite, coalified root traces or other features indicative of saturation during soil development.

Upper Paleosol Interval.—The UPI was initially well-drained (probably during sea level lowstand) and formed in a dry (~700 mm/yr), but seasonal climate as suggested

by oxidized soil colors, illuviated clay accumulations, pedogenic calcite nodules, and b-fabrics (Figs. 4A, 5B, H, 6). The climate became markedly more humid for the remainder of LPI formation (~1300mm/ yr; Fig. 6), but vertic features are pervasive throughout and indicate sustained seasonality (Figs. 4A, 5, 12). A fine-grained sandstone BCg horizon with relict bedding structures divides the UPI into two paleosol profiles, and the pedofeatures in the upper profile differ from those observed in the profile below (Fig. 4A). Above the sandstone, the interval neither contains pedogenic calcite nodules nor illuviated clay, but instead shows evidence for poor drainage such as gley colors, coalified root traces, and pedogenic siderite (Figs 4A, 5F). The pervasive nature of the gleying and the lack of pedogenic calcite or illuviated clay seem to indicate that the gleying in the upper part of the UPI was a result of regional water-table rise creating reducing conditions, and not simply overprinting due to marine hydromorphism during transgression (Fig. 4A, 12). The presence of pedogenic siderite supports this conclusion because it is known to form in poorly drained soils under low Eh and moderate pH conditions as a result of microbially mediated processes (Fig. 5F, Ludvigson et al. 1998; Driese et al. 2010). Gley matrix colors indicate that Fe was reduced as a result of poor drainage, and pedotransfer function results suggest that the pH was near neutral making conditions appropriate for siderite precipitation (Fig. 5F, 8E). The pedogenic siderite appears to pseudomorph root channels and it is possible that decaying root material served as a metabolite for the microbes that facilitated precipitation of siderite (e.g. Driese et al. 2010; Fig. 5F).

Overall Trends.—Overall trends indicate increasing seasonality of precipitation during the formation of the LPI and highly seasonal precipitation throughout the formation of the UPI and (Figs. 11, 12). These findings are consistent with other

paleoclimate studies from the western coast of Pangea during the late Pennsylvanian that give evidence for a monsoonal climate caused by the presence of the Central Pangean Mountain chain (Tabor and Montañez 2002, 2004; Tabor and Poulsen 2008). The results of the CALMAG paleoprecipitation proxy show considerable variability during the formation of both paleosol intervals (Figs. 11, 12). The UPI shows evidence for high water-table levels probably associated with gradual sea-level rise during transgression, whereas the LPI displays evidence of dominantly good drainage during formation, succeeded by late-stage, top-down overprinting of gley features following a more rapid transgression (Figs. 11, 12).

Clay Mineralogy and Soil Fertility

Pedotransfer function results indicate high clay and fine clay percentages, and high COLE values, all of which suggest the paleosols were originally dominated by high shrink-swell clays (Figs. 8, A, B, C). Vertic features throughout both profiles also point to a clay mineralogy initially dominated by smectite (Figs. 4A, B, 5A, B, C, H). Diagenetic alteration converted smectite to illite via temperature, pressure, and time (Fig. 8; Mora et al. 1998; Retallack 2001).

Smectite has a high cation-exchange-capacity compared to other clay types (80-120 cmolc/kg; Brady and Weil 2002). A dominantly smectite clay mineralogy combined with high base saturation, and neutral pH estimates indicates that these paleosols had a high cation exchange capacity (CEC) and would have readily supported plant growth (Figs. 8D, E, G). The reconstructed EC values are below 4 dS/m, and ESP values are below 15% throughout both profiles indicating that there were no problems with soil salinization (Figs. 8H, I; Brady and Weil 2002). The general good agreement of the

pedotransfer function results with those measured in the League series Vertisol lend support to the utility of these proxies in the deep time paleosol record (Fig. 7).

Paleoatmospheric PCO₂

The paleoatmospheric pCO₂ estimates from the Brownwood Spillway paleosols indicate levels at or near preindustrial levels (Fig. 10). These results are in agreement with other published proxy and modeling results from the same time period, and can be interpreted with greater confidence based on recent work that better constrains the appropriate S(z) value for paleosols with vertic properties (Breecker et al. 2013; Montañez 2013). The influence of pCO₂ variations on earth surface temperature is recognized as being one of a number of important factors controlling precipitation on equatorial Pangea (Peyser and Poulsen 2008). Global climate modeling results indicate that low pCO₂ results in less continental heating, greater soil moisture, and increased precipitation over low-latitude Pangea, which is consistent with the findings from this study (Peyser and Poulsen 2008).

CONCLUSIONS

The Lake Brownwood Spillway paleosols record a complex history of changes in soil hydrology, and precipitation as influenced by changing climate conditions and glacioeustatically driven sea-level changes. Both paleosol intervals formed in a dynamic fluvial-deltaic setting on the eastern margin of the Midland Basin, but record different climatic and hydrologic histories. (1) The LPI formed under a precipitation regime that was initially humid (~1300 mm/yr), but minimally seasonal (Figs. 4B, 5D, 6), followed by a drier (~680 mm/yr) and more seasonal climate phase (Figs. 4B, 6), and finally a

wetter (~1400 mm/yr) and highly seasonal phase (Figs., 4B, 6, 11). (2) The LPI was better-drained (at least seasonally) for the duration of its formation, but following transgression, the uppermost horizon of the LPI was overprinted by gley features via top-down marine hydromorphism (e.g. Driese and Ober 2005; Fig. 4B, 11). (3) MAP estimates for the UPI show an increase from initially dry (~700mm/yr) to more humid conditions (~1300mm/yr), and well-developed vertic features throughout indicate that precipitation was highly seasonal for the duration of its formation. The UPI started out well-drained, but drainage became increasingly poor through time likely due to a long-term regional rise in water-table levels. (4) The upper and lower paleosol intervals represent complex, but different paleohydrologic and paleoclimatic histories. This study demonstrates that, in spite of the presence of multiple episodes of overprinting during soil formation, careful field and micromorphological observations make it possible to decipher a complex history of changes in climate and soil hydrology. (5) Interpretations of a highly seasonal climate on the west coast of Pangea during the late Pennsylvanian are in agreement with other paleosol studies, and paleoclimate computer modeling results (Tabor and Montañez 2002, 2004; Tabor and Poulsen 2008). (6) Pedotransfer function results indicate these paleosols were clay-rich, fertile, and free of salinity or nutrient deficiency problems, and thus would have readily supported plant growth. The proxy results compare well with the directly measured values from the modern analog League series Vertisol. These findings demonstrate the utility of these proxies in paleosols as old as late Pennsylvanian, and provide important insights into the physical and biochemical conditions that existed pre-diagenesis. (7) Paleatmospheric pCO₂ estimates using the paleosol calcite paleobarometer average 360 ppmV, which are in agreement with other

published proxy and computer modeling data and appropriate values for late Pennsylvanian icehouse conditions (Fig. 10).

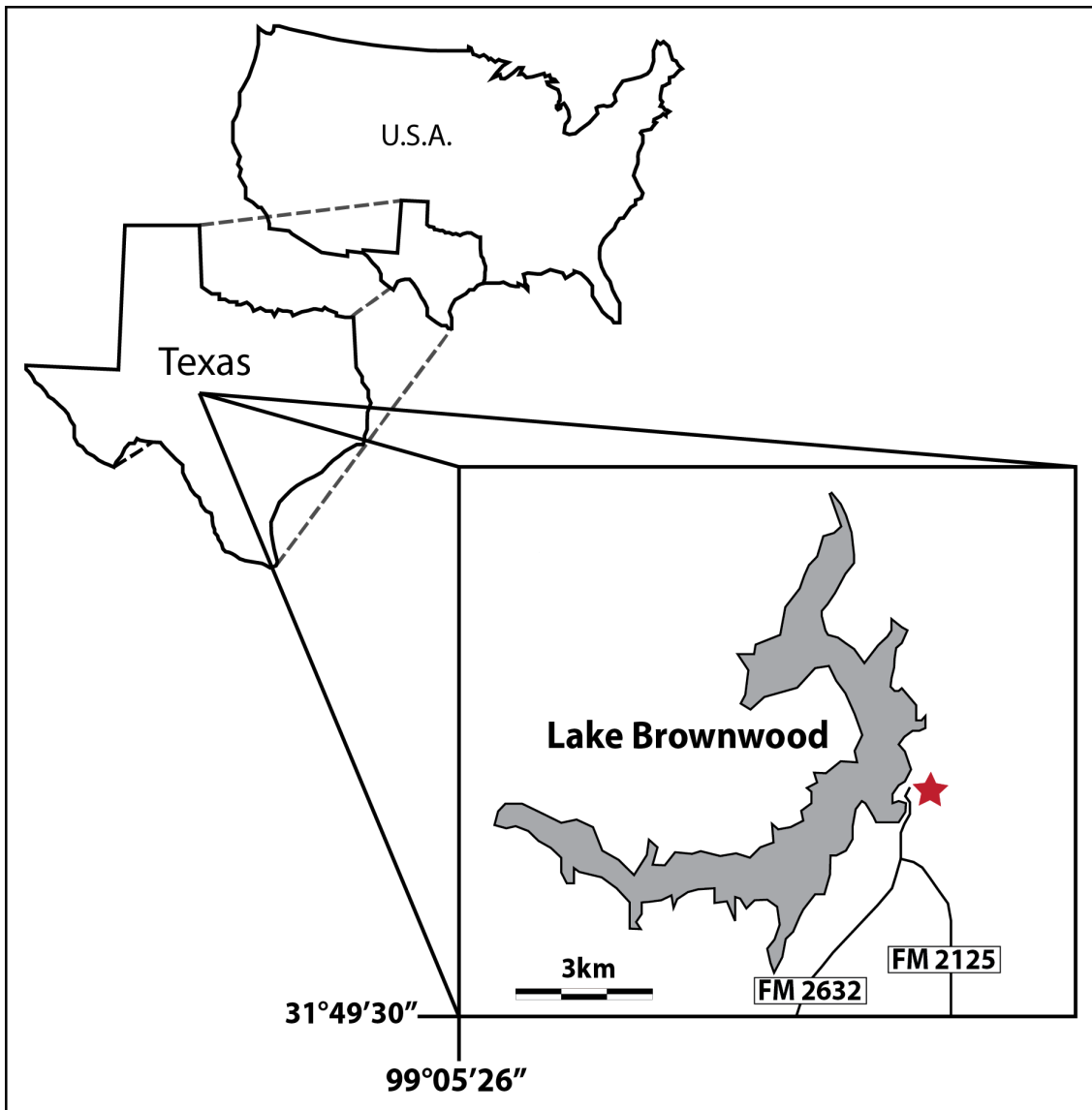


Figure 1. Location map of the Lake Brownwood Spillway study area in north-central Texas, USA.

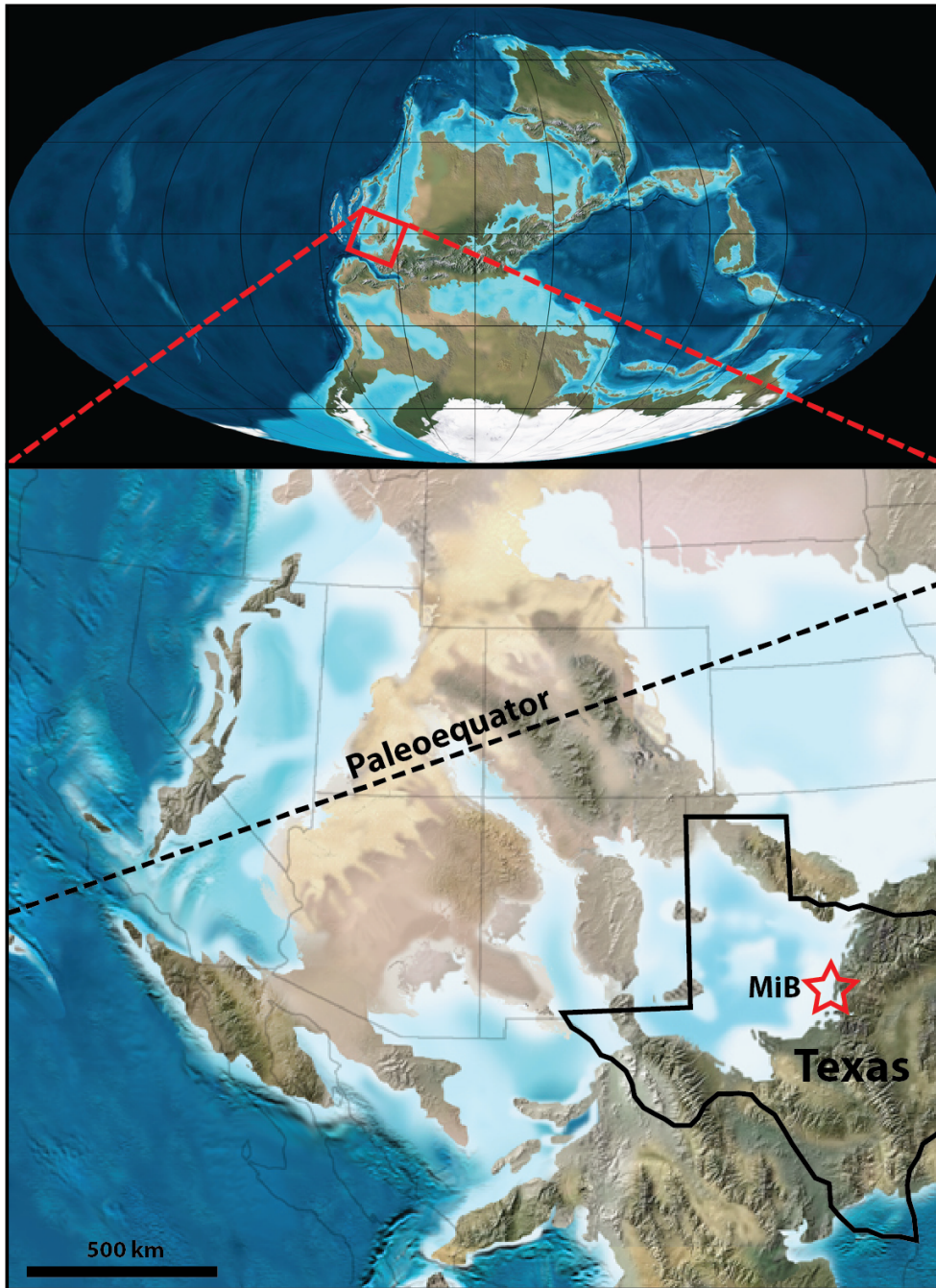


Figure 2. Paleogeographic map showing the study location on the margin of the Midland Basin (MiB), and approximate location of the paleoequator during the late Pennsylvanian (Modified from Blakey, 2003, and 2011).

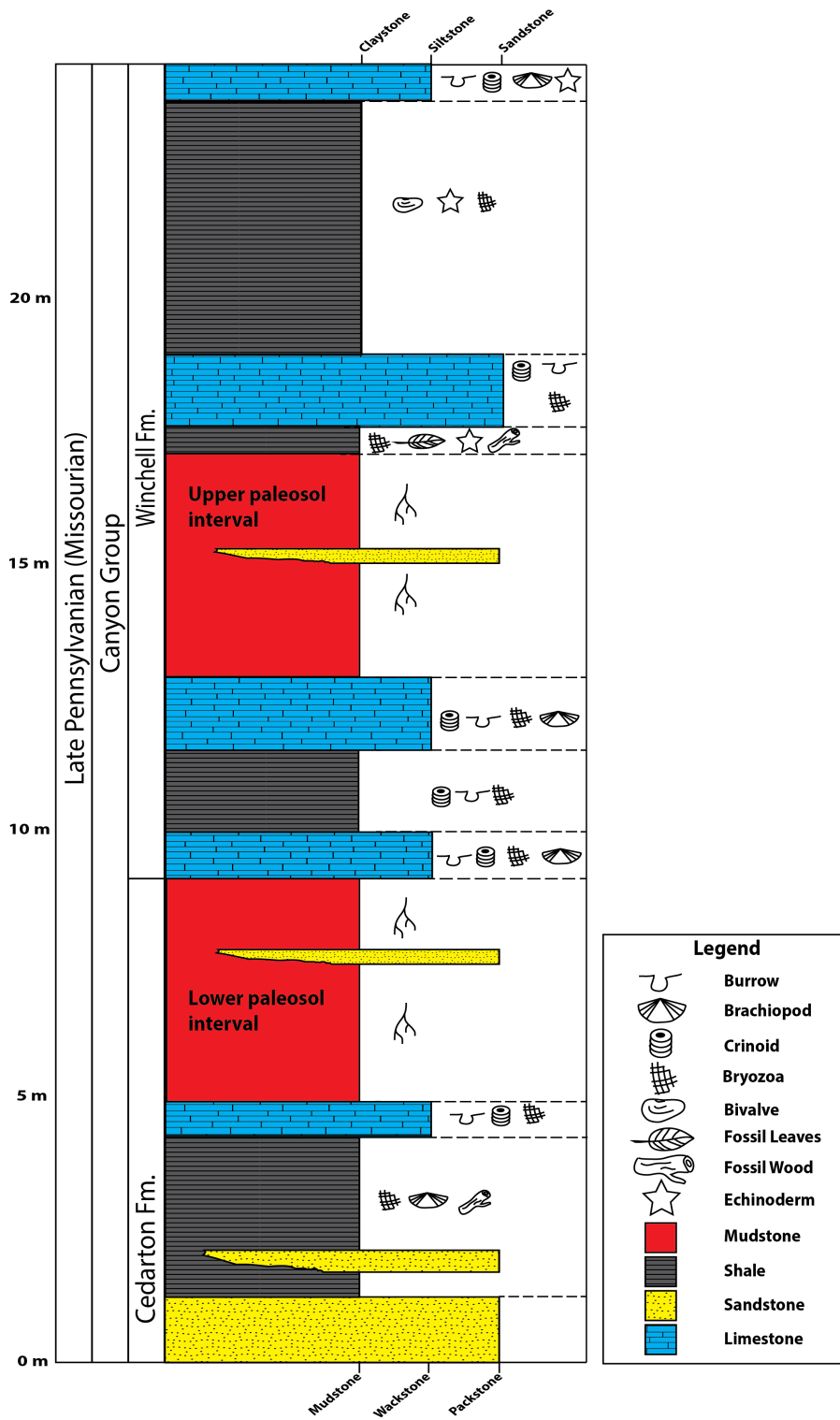
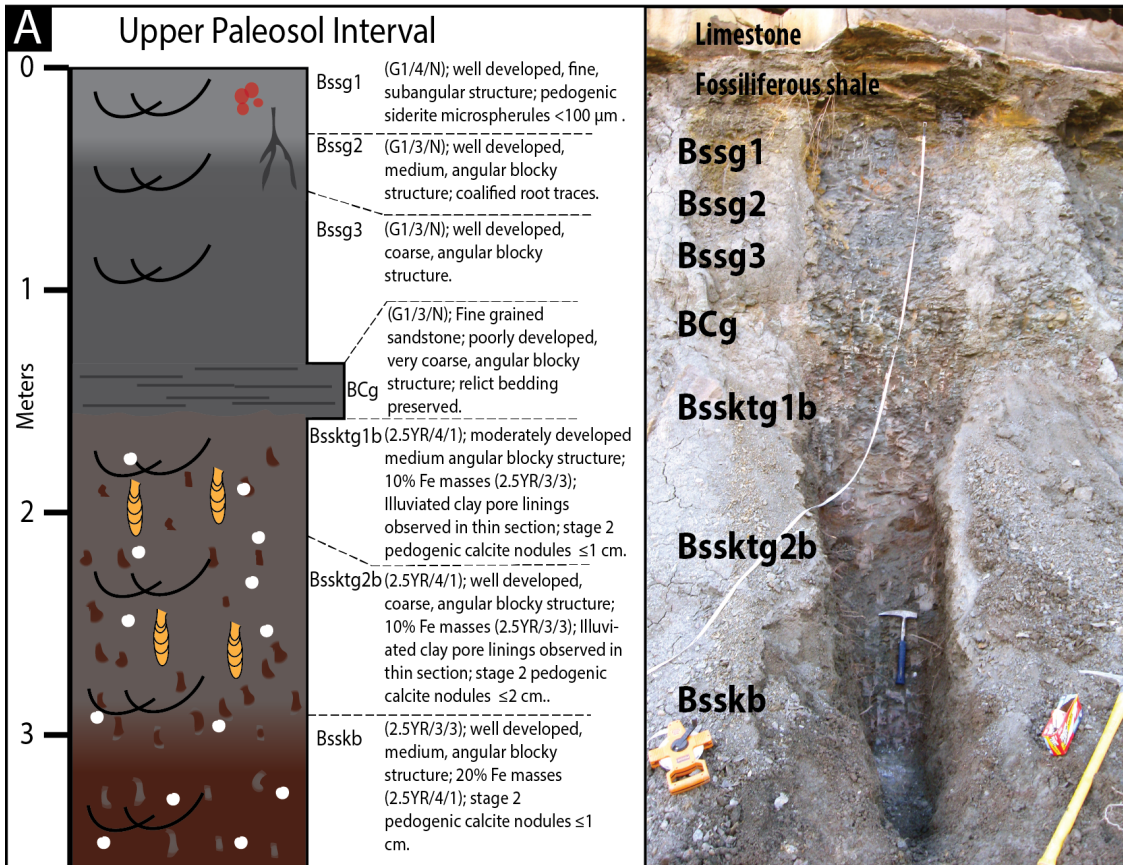


Figure 3. Stratigraphic section from the Lake Brownwood Spillway. Note the locations of the Upper paleosols interval (UPI) and Lower paleosol interval (LPI). See text for discussion.



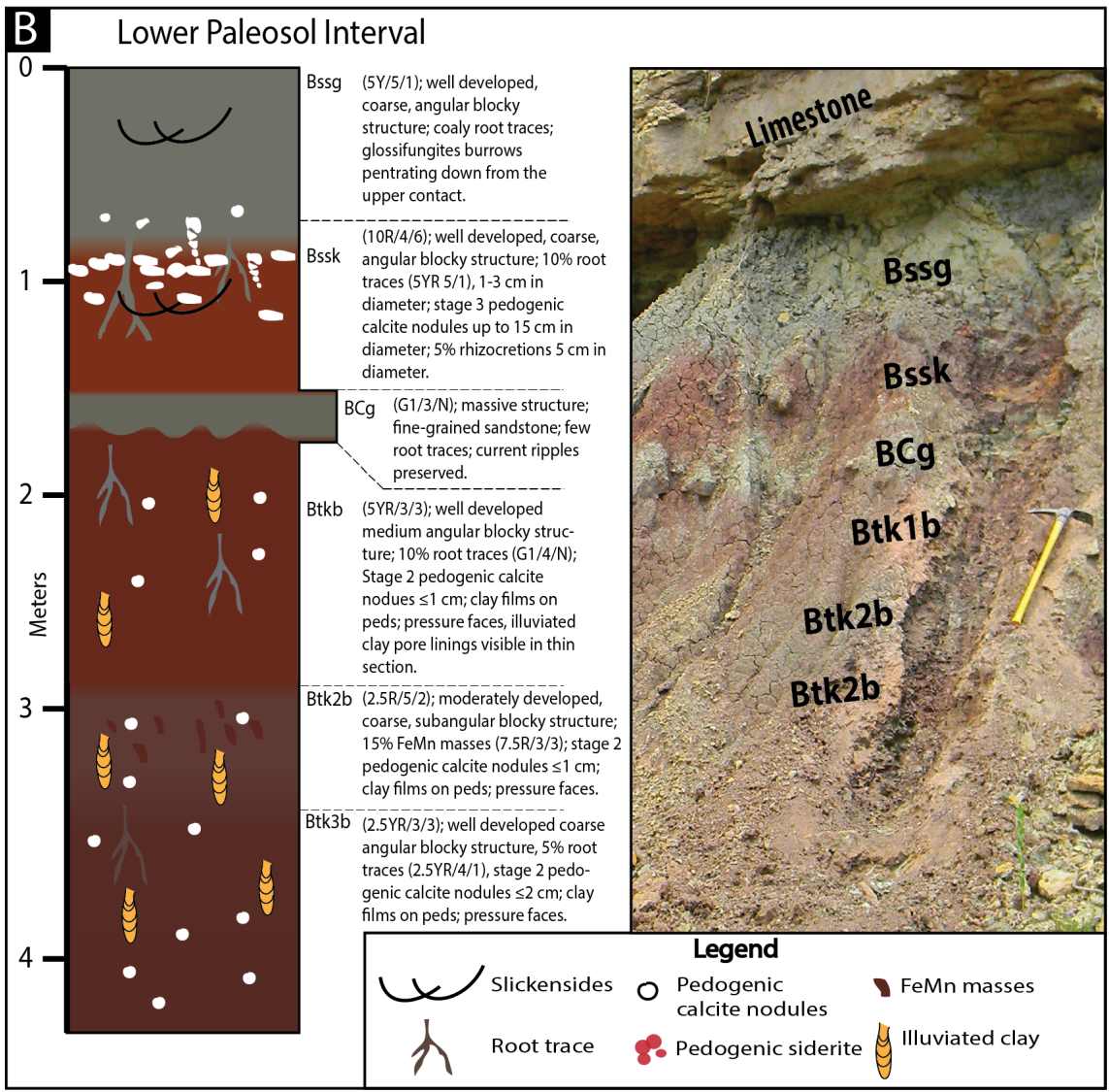


Figure 4. Outcrop sections of the Upper (UPI: A) and Lower (LPI: B) Paleosol Intervals at Lake Brownwood Texas showing horizon designations and field descriptions along with corresponding field photographs.

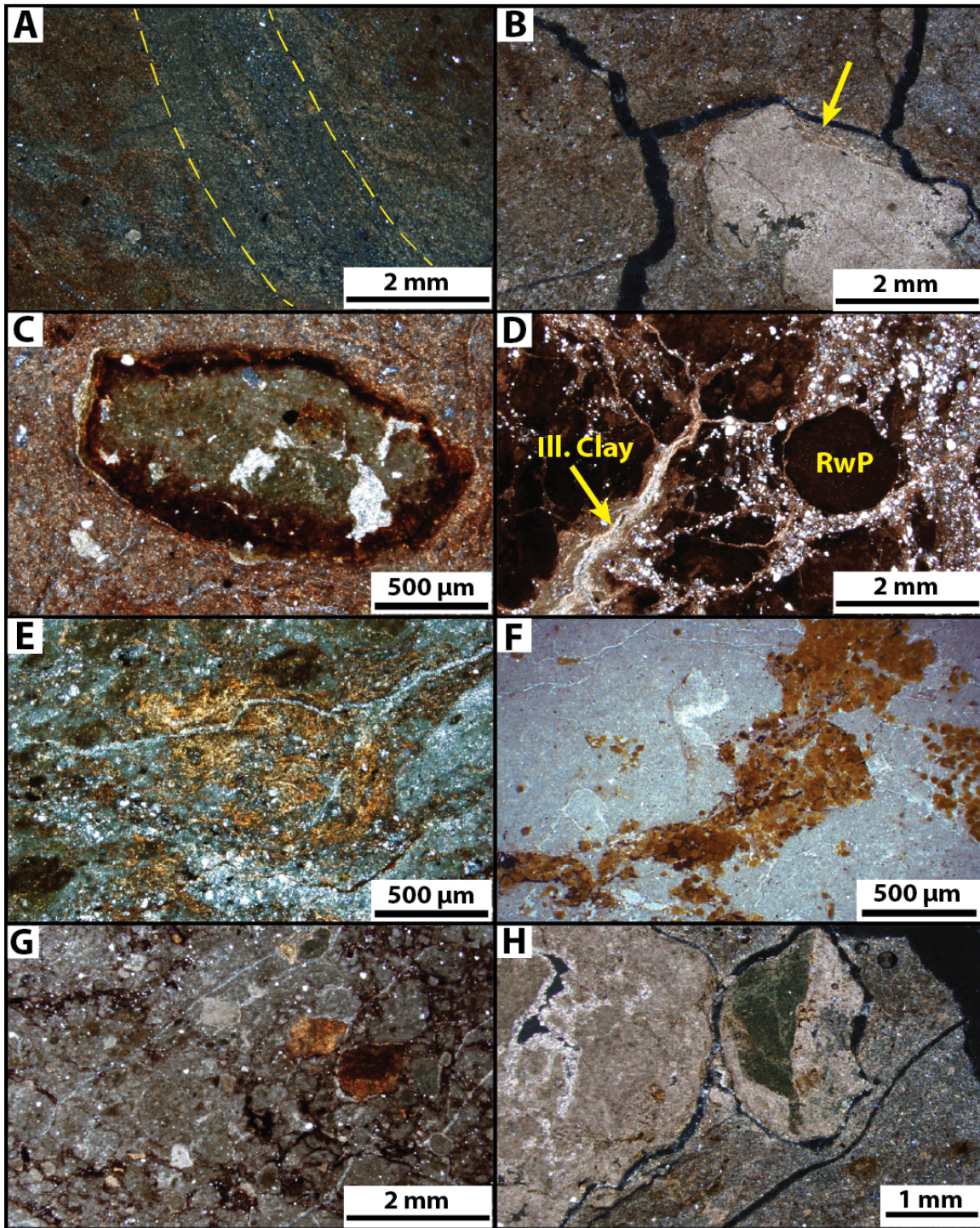


Figure 5. Thin-section photomicrographs show pedogenic features from the UPI and LPI. All photos were taken under cross-polarized light except for (F). (A) Redox depletion root channel (outlined with dashed yellow lines) in an oxidized matrix with parallel striated b-fabric, 80 cm depth, LPI. (B) Pedogenic calcite nodule with septarian shrinkage cracks surrounded by granostriated b-fabric (yellow arrow), 320 cm depth, UPI. (C) Pedogenic calcite nodule with FeMn corrosion rim, 80 cm depth, LPI. (D) Reworked peds (RwP) in a fine sandy matrix crosscut by illuviated clay pore-linings (Ill. Clay), 200 cm depth, LPI. (E) Illuviated clay pore-filling, 235 cm depth, LPI. (F) Pedogenic siderite microspherules associated with organic matter and filling a paleo root channel, 30 cm depth, UPI. (G) Reworked peds, pedogenic calcite nodules, and clay

papules (golden color; reworked illuviated clay skins), with FeMn oxide concentrations, 185 cm depth, UPI. **(H)** Two pedogenic calcite nodules with grano-striated b-fabric. The one on the right has an inherited calcite core; the one on the left has septarian shrinkage cracks lined with sparry calcite, 280 cm depth, UPI.

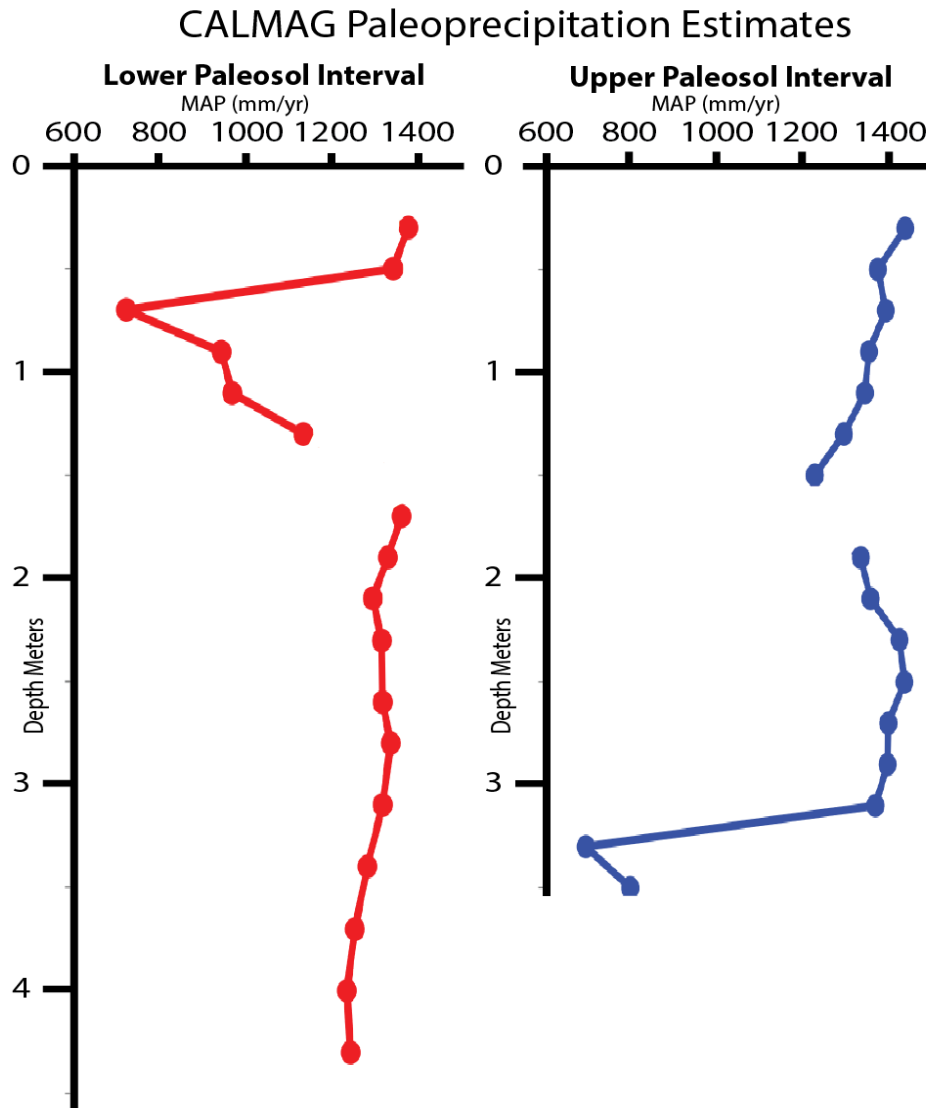


Figure 6. Paleoprecipitation estimates using the CALMAG paleoprecipitation proxy calibrated for vertic paleosols (Nordt and Driese, 2010a). Note that gaps in data are where sandy horizons without vertic features exist that do not meet the criteria for application of the CALMAG proxy.

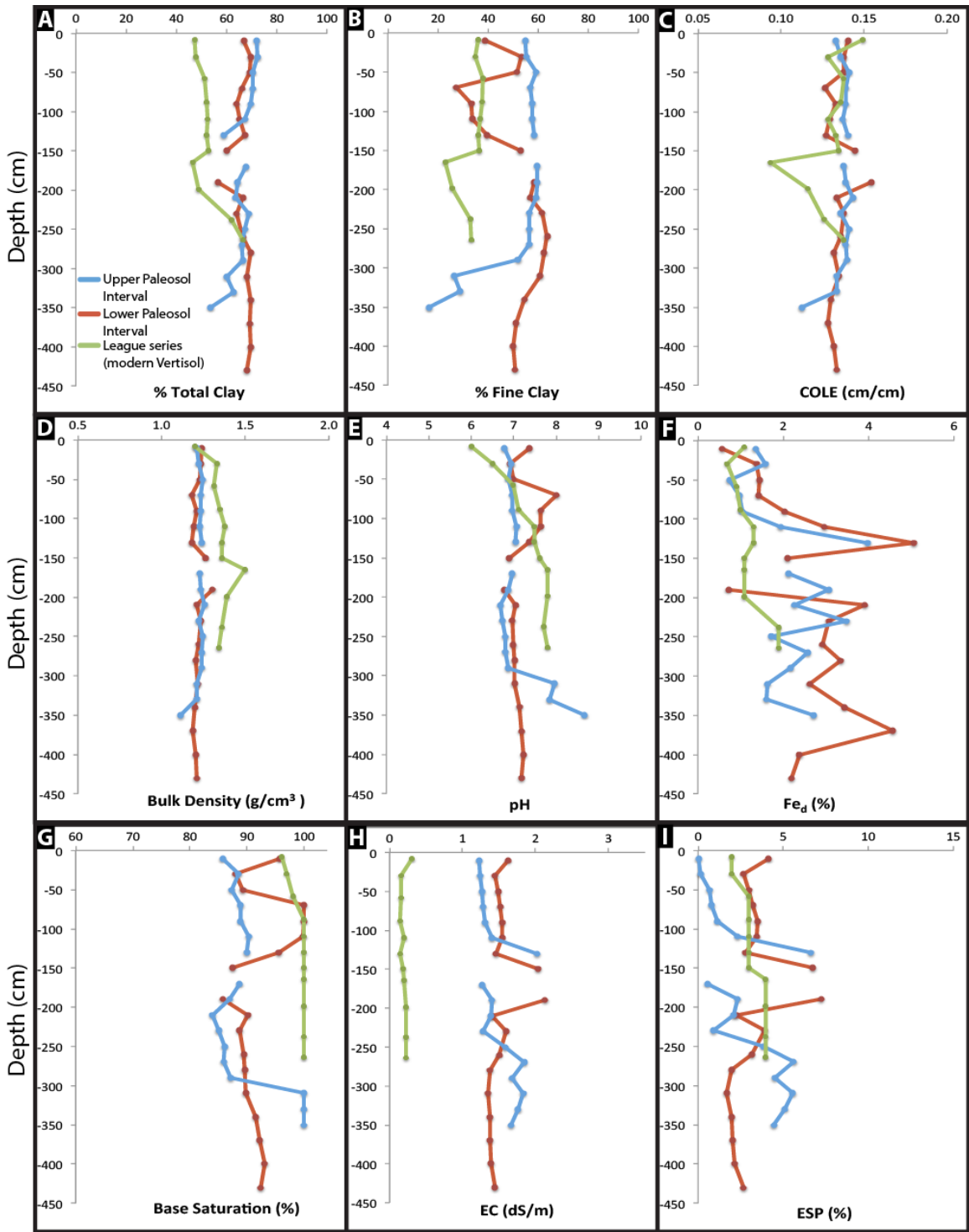


Figure 7. Reconstructed physical and chemical properties of the Lake Brownwood Spillway paleosols compared to measured values from the League series Vertisol, Jefferson County Texas, USA.

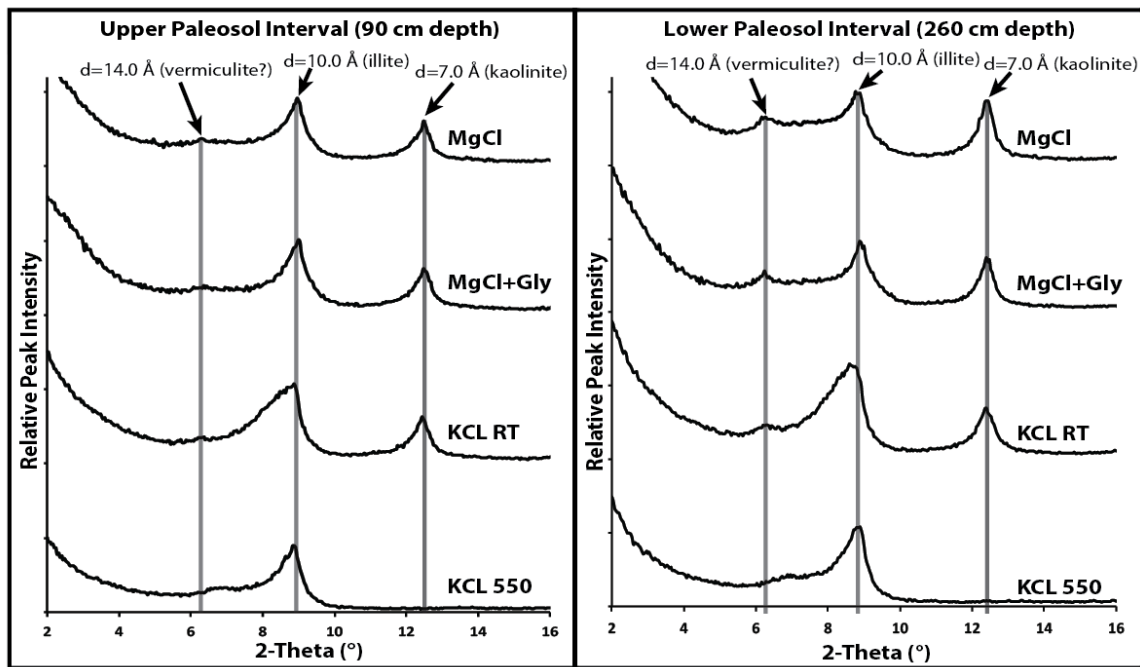


Figure 8. X-ray diffraction patterns from the Bssg3 horizon of the UPI at 90 cm depth, and the Btkb horizon of the LPI at 260 cm depth. Note the collapse of the 7.0 Å peak, and the slight shift of the 14.0 Å peak after having been heated to 550° C.

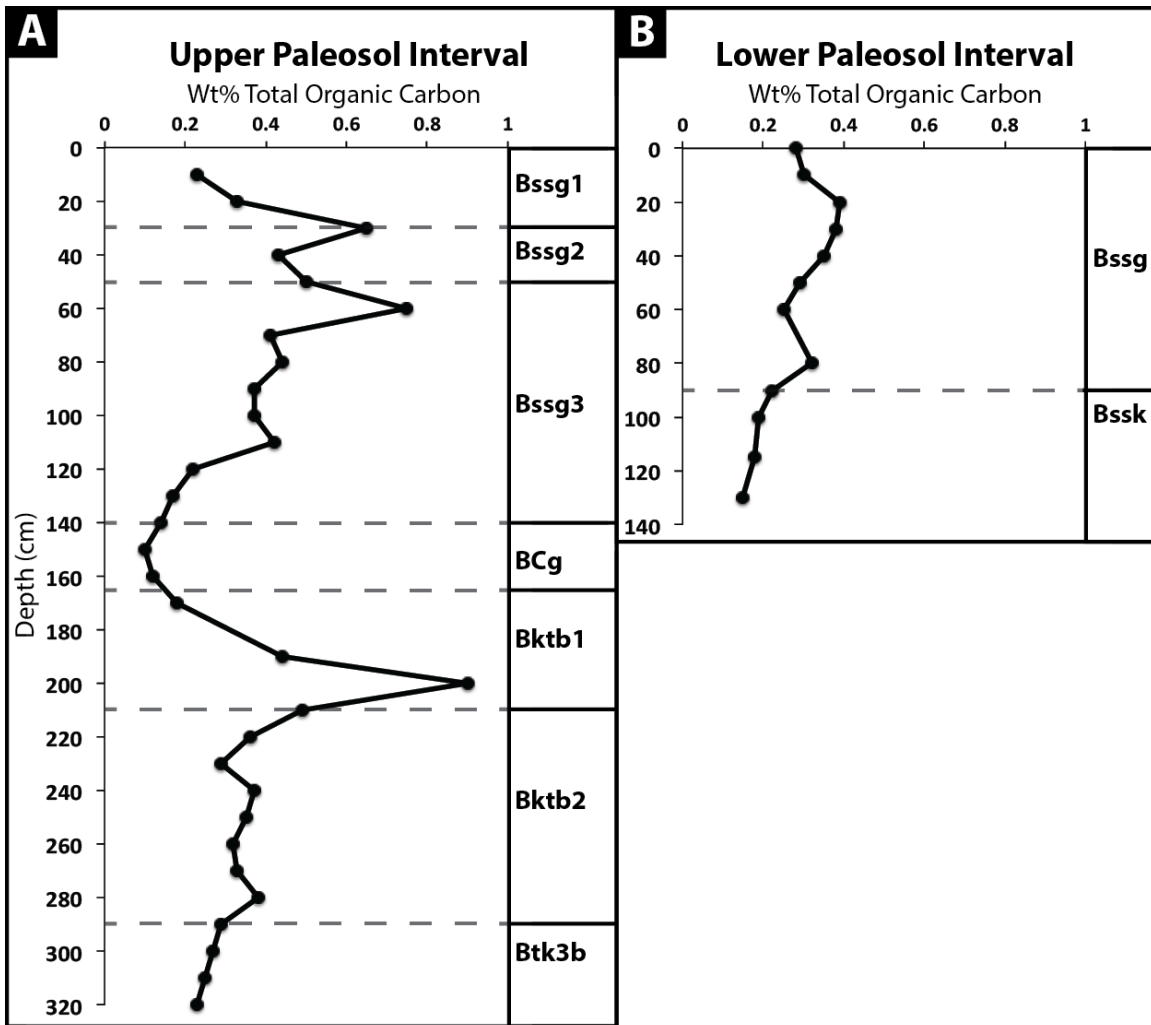


Figure 9. Weight percent total organic carbon (TOC) values in the UPI (A) and LPI (B) with corresponding horizon designations. Note that TOC data were not collected below 130 cm depth in the LPI.

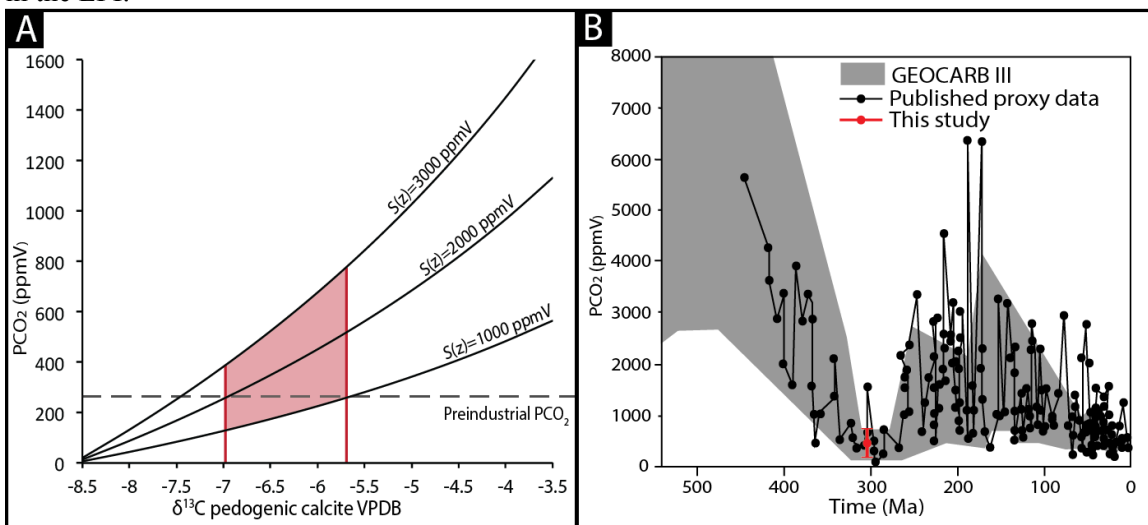


Figure 10. (A) Paleatmospheric pCO₂ estimates calculated using the $\delta^{13}\text{C}$ of pedogenic calcite nodule from both paleosol intervals and an assumed range of 1000 to 3000 ppmV for S(z). (B)

Results from this study compared to other published proxy data and the GEOCARB III computer model for paleoatmospheric $p\text{CO}_2$ (modified from Royer, 2006).

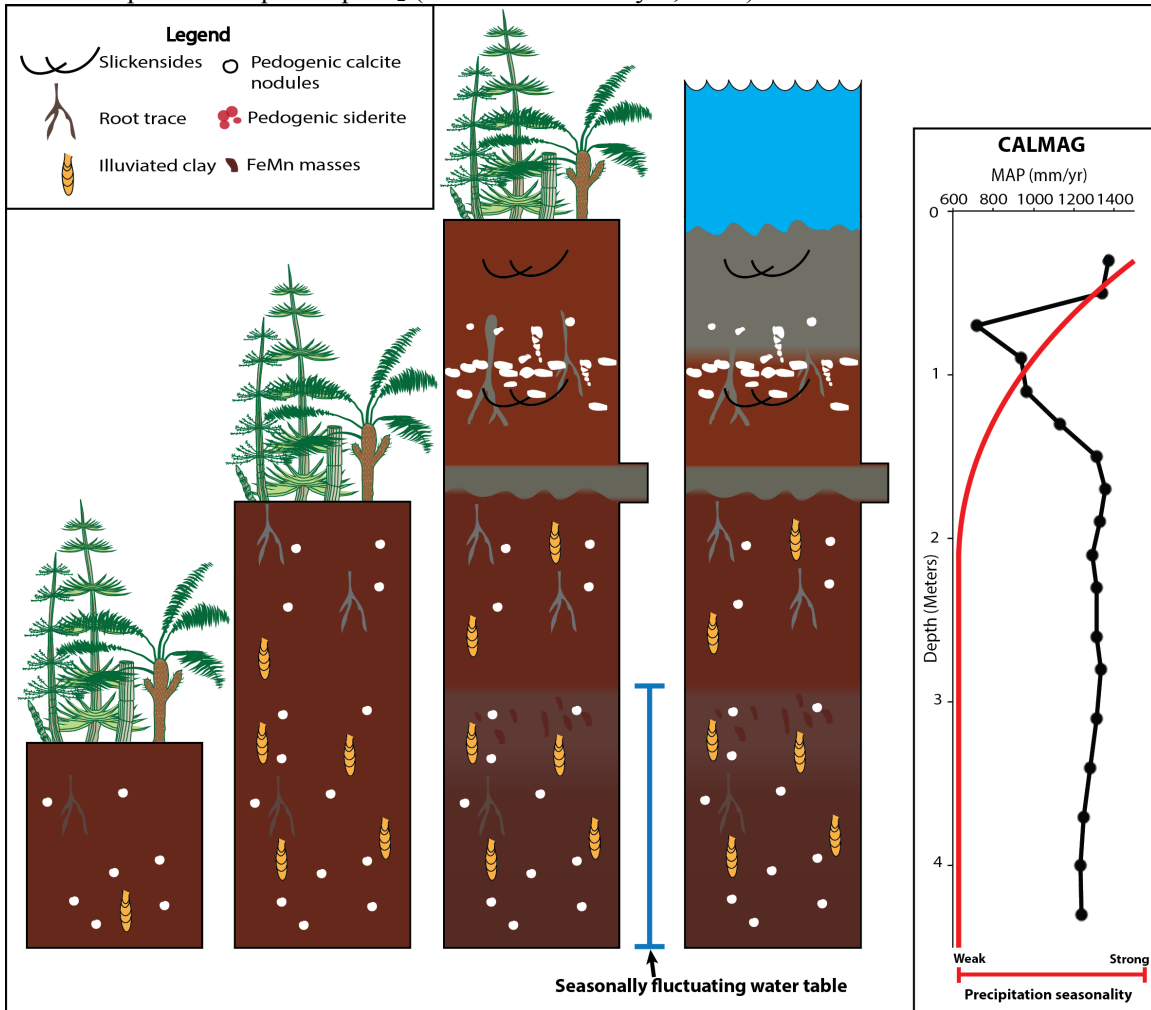


Figure 11. Proposed paleohydrologic and paleoprecipitation model for the LPI including CALMAG paleoprecipitation estimates. The soil was initially well-drained and precipitation seasonality is minimal with CALMAG paleoprecipitation estimates of ~ 1200 mm/yr. The climate became drier (~ 700 mm/yr) and more seasonal, and the subsoil was saturated periodically during times of the year when the water table is high. Finally, precipitation rates increased to ~ 1300 mm/yr prior to submergence and gleying during transgression.

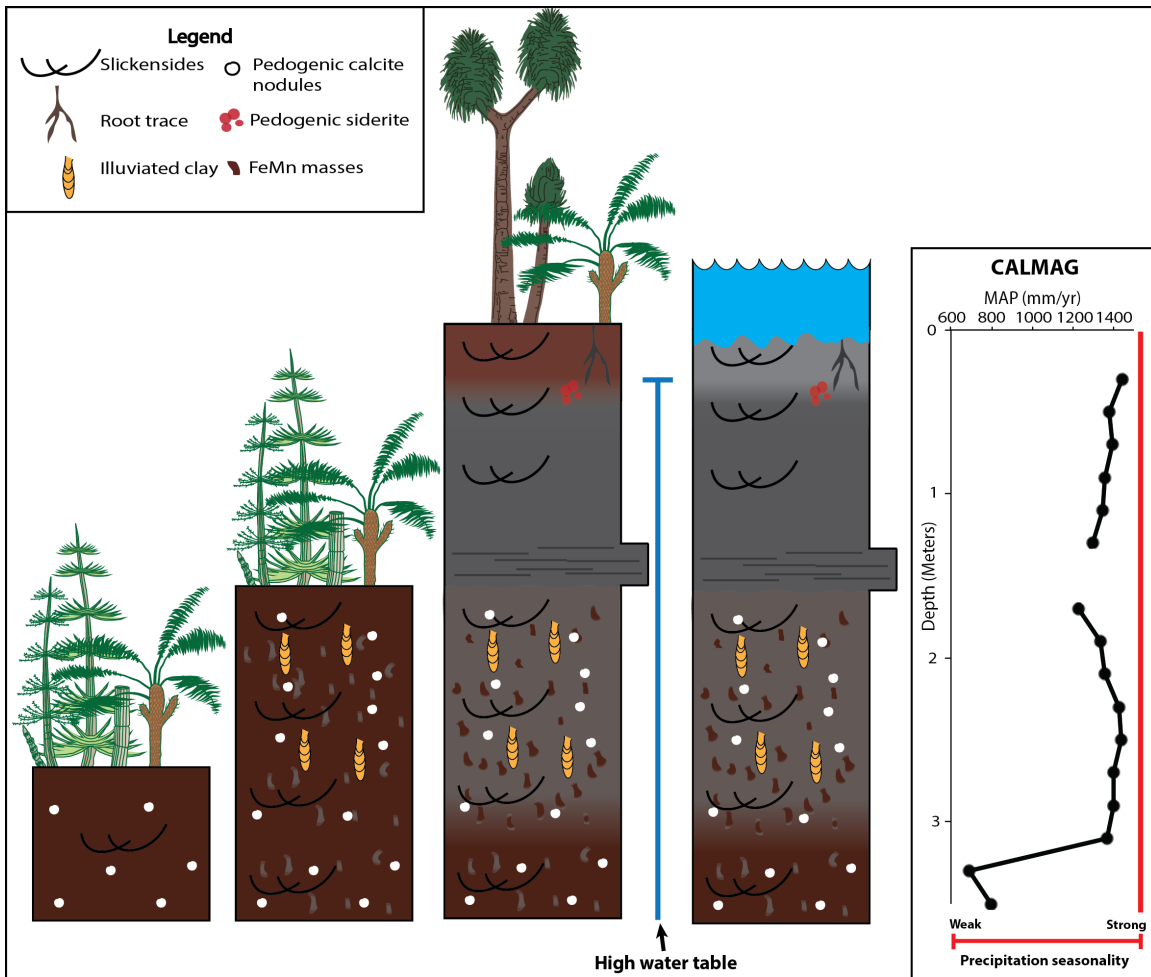


Figure 12. Proposed paleohydrologic and paleoprecipitation model for the UPI including CALMAG paleoprecipitation estimates. The soil was initially well-drained in dry seasonal climate. Precipitation rates increased markedly but soil drainage was still good. A regional water-table rise resulted in overprinting of gley features and dominantly (not permanently) saturated soil conditions. Lastly, sea level rise resulted in further gleying, and precipitation of siderite during saturated conditions. See

Property*	Horizont†	Molecular oxide§	Equation	r ²	RMSE
Clay	Noncalcareous	Al ₂ O ₃	y = 3.965x + 3.681	0.74	± 4
Clay	All, <5%CaO	Al ₂ O ₃	y = 3.118x + 15.22	0.62	± 5
Clay	All, <10% CaO	Al ₂ O ₃	y = 2.434x + 23.08	0.42	± 6
Fine clay	All, <10% CaO	Al ₂ O ₃ /(CaO + MgO)	y = 9.975ln(x) + 23.68	0.48	± 7
COLE	Noncalcareous	CaO + MgO	y = 1.345x + 0.077	0.49	± 0.019
COLE	Calcareous, <10% CaO	SiO ₂	y = 0.00238x - 0.02965	0.31	± 0.025
Bulk density	Noncalcareous	SiO ₂	y = 0.011x + 0.457	0.27	± 0.10
pH	All, <30% CaO	CaO + MgO	y = 0.871ln(x) + 9.648	0.67	± 0.6
Base saturation	All, <30% CaO	CaO + MgO	y = 14.69ln(x) + 134.0	0.73	± 8
Fe_d	All, <30% CaO	Fe ₂ O ₃	y = 0.085x ² - 0.352x + 0.658	0.78	± 0.4
ESP	All, <10% CaO	Na ₂ O/Al ₂ O ₃	y = 110.4x - 2.935	0.77	± 4
EC	All, <10% CaO	Na ₂ O/Al ₂ O ₃	y = 290.7x ² + 24.33x + 1.145	0.72	± 3

Table 1. Pedotransfer functions of Nordt and Driese (2010b) (table modified to only include those used in this study) *COLE—coefficient of linear extensibility; Fe_d—dithionite citrate extractable Fe; ESP—exchangeable sodium percentage; EC—electrical conductivity. †“Noncalcareous” includes only noncalcareous horizons; “all” includes noncalcareous and calcareous horizons combined; “calcareous” includes only calcareous horizons. § Expressed as weight percentage, but on a molecular oxide basis when more than one element is used in the regression equation.

CHAPTER THREE

Conclusions

This study provides more detailed climatic records from the western Pangea during the late Pennsylvanian and shows that in spite of polygenesis in paleosols, high resolution climatic records can be obtained through careful micromorphological, micromorphological and geochemical techniques. This study also shows that pedotransfer functions can be used to reconstruct physical and colloidal properties of Paleozoic paleosols, which provides invaluable information about past ecosystems. These findings contribute to the body of knowledge on the late Paleozoic ice age, which is an excellent analog for global conditions and could provide valuable information about the future of climate change.

APPENDIX A

Table A.1
Bulk geochemical data

Lower paleosol interval		Recvd Wt.	Ag	Al	Al ₂ O ₃	As	Ba	Be	Bi	Ca	CaO	Cd
Horizon	Depth (cm)	kg	ppm	%	wt %	ppm	ppm	ppm	ppm	%	wt %	ppm
Bssg	10	0.04	0.03	8.77	16.57	1.5	270	3.54	0.37	1.46	2.04	0.02
"	30	0.04	<0.01	9.26	17.50	3.2	150	3.71	0.26	0.35	0.49	<0.02
"	50	0.04	<0.01	9.17	17.33	2	190	3.74	0.19	0.42	0.59	<0.02
Bkss	70	0.04	<0.01	8.61	16.27	0.5	190	2.94	0.19	4.52	6.32	0.03
"	90	0.04	<0.01	8.28	15.64	3.6	170	3.44	0.25	2.41	3.37	<0.02
"	110	0.04	0.02	8.51	16.08	4.3	190	3.79	0.25	2.31	3.23	<0.02
"	130	0.04	0.02	8.81	16.65	2.8	230	3.81	0.32	1.34	1.87	<0.02
BCg	150	0.04	0.02	7.63	14.42	1.8	270	2.92	0.31	0.31	0.43	<0.02
Btkb	170	0.04	0.01	6.24	11.79	3.2	300	1.66	0.19	0.19	0.27	<0.02
"	190	0.04	0.07	7.01	13.25	1.7	270	1.96	0.23	0.16	0.22	<0.02
"	210	0.04	0.08	8.68	16.40	3.4	340	2.84	0.35	0.23	0.32	<0.02
"	230	0.04	0.08	8.3	15.68	2.7	320	2.67	0.32	0.14	0.20	<0.02
"	260	0.04	0.09	8.69	16.42	3.4	350	2.82	0.34	0.12	0.17	<0.02
Btk2b	280	0.04	0.09	9.21	17.40	4.6	330	3.72	0.41	0.14	0.20	<0.02
"	310	0.04	0.08	8.96	16.93	5.9	300	3.88	0.37	0.16	0.22	<0.02
Btk3b	340	0.04	0.07	9.23	17.44	6.9	310	4.03	0.37	0.32	0.45	<0.02
"	370	0.04	0.09	9.13	17.25	6.4	300	3.91	0.36	0.43	0.60	<0.02
"	400	0.04	0.08	9.2	17.38	4	300	3.88	0.32	0.49	0.69	<0.02
"	430	0.04	0.09	8.99	16.99	3.6	300	4.15	0.34	0.44	0.62	<0.02
R (limestone)	460	0.04	0.04	2.66	5.03	<5	90	0.85	0.17	20.2	28.26	1.27

Lower paleosol interval		Ce	Co	Cr	Cs	Cu	Fe	Fe2O3	Ga	Ge	Hf	In	K
Horizon	Depth (cm)	ppm	ppm	ppm	ppm	ppm	%	wt %	ppm	ppm	ppm	ppm	%
Bssg	10	79.7	20.1	92	10.9	9.1	2.72	3.89	23.3	0.21	3.5	0.072	2.52
"	30	56.1	8.9	90	14.1	60.3	3.94	5.63	22.3	0.24	3.3	0.081	2.69
"	50	142.5	10.7	86	15.55	53.7	4.02	5.75	22.9	0.36	3.3	0.073	2.61
Bkss	70	54	9.7	78	13.3	5.6	3.99	5.70	21.3	0.21	3.1	0.076	2.48
"	90	49.5	10.3	78	11.8	41.2	4.61	6.59	21.1	0.24	3	0.073	2.55
"	110	49	10.5	82	12.05	34.5	5.38	7.69	22.1	0.22	3.1	0.084	2.59
"	130	64.4	12.4	80	10.75	21.8	6.69	9.56	23.4	0.3	3.1	0.085	2.59
BCg	150	89.2	12.2	64	7.86	26.7	4.67	6.68	19.1	0.28	3.6	0.06	1.99
Btkb	170	76.6	9.5	49	5.39	25.6	2.08	2.97	15.8	0.08	3.8	0.047	1.57
"	190	83.2	11.7	57	7.33	37.3	2.99	4.27	18.85	0.13	3.5	0.056	1.86
"	210	86.1	14.6	77	10.45	28.6	6.01	8.59	25.9	0.2	3.1	0.073	2.51
"	230	74.3	15	75	9.25	30.6	5.44	7.78	25.2	0.19	3.2	0.074	2.36
"	260	102	14.1	73	10.45	29.4	5.33	7.62	24.4	0.18	3.4	0.073	2.5
Btk2b	280	59.8	13.8	89	10.55	28.4	5.64	8.06	28	0.21	3.2	0.079	2.9
"	310	50.2	14.6	88	10.55	34.4	5.1	7.29	27.3	0.19	3.1	0.085	2.84
Btk3b	340	39	16.7	93	10.25	27.7	5.7	8.15	29.4	0.21	3.1	0.081	3.02
"	370	41.1	15.5	90	10.2	21.2	6.41	9.16	28	0.22	3.1	0.08	2.99
"	400	52.4	14.2	88	11	19.4	4.92	7.03	26.6	0.19	3.3	0.085	3.06
"	430	42.3	15.4	88	10.1	19.4	4.75	6.79	27.2	0.19	3.4	0.08	3.04
R (limestone)	460	67.5	5.1	22	2.18	7.3	1.4	2.00	6.74	0.12	1.7	0.058	0.71

Lower paleosol	K2O	La	Li	Mg	MgO	Mn	MnO	Mo	Na	Na2O	Nb	Ni
----------------	-----	----	----	----	-----	----	-----	----	----	------	----	----

interval													
Horizon	Depth (cm)	wt %	ppm	ppm	%	wt %	ppm	wt %	ppm	%	wt %	ppm	ppm
Bssg	10	3.04	37.3	34.6	0.9	1.49	0.0099	0.0128	0.33	0.48	0.647	15.6	49.4
"	30	3.24	24.3	26.3	0.85	1.41	0.0046	0.0059	0.48	0.4	0.539	14.9	29.6
"	50	3.14	60.3	28.2	0.9	1.49	0.0071	0.0092	0.37	0.42	0.566	15.5	37.8
Bkss	70	2.99	25.4	32.6	0.99	1.64	0.0243	0.0314	0.23	0.41	0.553	14.6	38.2
"	90	3.07	22.4	34.9	0.96	1.59	0.0148	0.0191	0.32	0.41	0.553	14.2	39.5
"	110	3.12	21.4	37.1	0.97	1.61	0.0155	0.0200	0.44	0.42	0.566	14.9	37.8
"	130	3.12	29.1	58.8	0.97	1.61	0.0123	0.0159	0.39	0.39	0.526	14.6	43.2
BCg	150	2.40	46	79.9	0.84	1.39	0.0096	0.0124	0.31	0.57	0.768	14	38.5
Btkb	170	1.89	39.7	50.1	0.63	1.04	0.008	0.0103	0.21	0.63	0.849	11.8	27.3
"	190	2.24	41.2	63.3	0.81	1.34	0.0096	0.0124	0.28	0.55	0.741	12.5	35.1
"	210	3.02	38	88.5	1.09	1.81	0.0116	0.0150	0.36	0.35	0.472	13.4	44.9
"	230	2.84	32.8	94.3	1.03	1.71	0.0108	0.0139	0.34	0.44	0.593	14.4	45.6
"	260	3.01	48.9	86.6	1.09	1.81	0.0112	0.0145	0.34	0.41	0.553	14.8	44.3
Btk2b	280	3.49	21.1	90.7	1.09	1.81	0.0102	0.0132	0.37	0.35	0.472	14	48.1
"	310	3.42	19.7	82.8	1.1	1.82	0.012	0.0155	0.47	0.32	0.431	14	49.1
Btk3b	340	3.64	14.7	85.2	1.15	1.91	0.0121	0.0156	0.5	0.35	0.472	14.8	52.1
"	370	3.60	15.3	81.6	1.16	1.92	0.0123	0.0159	0.46	0.35	0.472	13.5	49.2
"	400	3.69	20.7	77.3	1.2	1.99	0.0123	0.0159	0.41	0.36	0.485	14.5	46.7
"	430	3.66	16.3	80.2	1.17	1.94	0.0121	0.0156	0.34	0.39	0.526	13.7	47.1
R (limestone)	460	0.86	32.5	20.6	1.07	1.77	0.248	0.3202	0.23	0.27	0.364	4.3	10.4

Lower paleosol interval													
Horizon	Depth (cm)	P	P2O5	Pb	Rb	Re	S	Sb	Sc	Se	Sn	Sr	Ta
		wt%	wt %	ppm	ppm	ppm	%	ppm	ppm	ppm	ppm	ppm	ppm

Bssg	10	0.046	0.105	9.3	167	<0.002	0.01	0.58	15.9	3	3.3	205	1.19
"	30	0.01	0.023	7.3	165.5	<0.002	0.01	0.94	17.2	2	3.4	195.5	1.11
"	50	0.032	0.073	6.6	192	0.002	0.01	0.92	16.6	3	3.3	212	1.14
Bkss	70	0.027	0.062	5.5	145.5	0.002	0.01	0.56	15.2	4	3.1	301	1.09
"	90	0.034	0.078	10	140.5	<0.002	0.02	1.19	14.9	3	3.2	296	1.05
"	110	0.036	0.082	14.5	147	0.002	0.02	1.64	16.1	3	3.3	250	1.09
"	130	0.04	0.092	15.3	137.5	0.002	0.01	1.55	15	3	3.6	237	1.11
BCg	150	0.036	0.082	9.2	127	<0.002	0.01	0.61	13.2	3	3	159	1.04
Btkb	170	0.019	0.044	6.1	101.5	<0.002	0.01	0.32	9.7	1	2.2	127.5	0.91
"	190	0.013	0.030	6.9	115	<0.002	<0.01	0.39	11.4	1	2.6	138	0.95
"	210	0.039	0.089	12.3	147.5	<0.002	0.01	0.79	17.3	1	3.4	180	1.11
"	230	0.019	0.044	10.3	131	<0.002	<0.01	0.72	16.7	1	3.3	174.5	1.09
"	260	0.017	0.039	11.3	159	<0.002	<0.01	0.85	17.4	1	3.5	174.5	1.15
Btk2b	280	0.017	0.039	14.1	137	<0.002	0.01	1.12	18.2	1	3.5	193.5	1.07
"	310	0.03	0.069	12.3	144.5	<0.002	0.01	1.02	17.9	1	3.5	191.5	1.04
Btk3b	340	0.034	0.078	13.4	133	<0.002	0.01	1.22	18.1	1	3.6	203	1.02
"	370	0.039	0.089	14	120.5	<0.002	<0.01	1.28	16.9	1	3.4	206	1.04
"	400	0.039	0.089	11.2	139.5	<0.002	0.01	0.97	17	1	3.7	199	1.14
"	430	0.039	0.089	10.7	125.5	<0.002	0.01	0.75	17.5	1	3.3	199	1.18
R (limestone)	460	0.016	0.037	8.8	39.2	<0.002	0.03	0.14	9.6	1	0.8	429	0.31

Lower paleosol interval		Th	Ti	TiO2	Tl	U	V	W	Y	Zn	Zr	Zr	SiO2
Horizon	Depth (cm)	ppm	%	wt %	ppm	ppm	ppm	ppm	ppm	ppm	ppm	wt %	wt%
Bssg	10	14.6	0.47	0.784	0.86	3.9	139	1.9	20.7	52	124	0.0124	71.40
"	30	12.9	0.462	0.771	0.98	1.8	114	1.9	13.4	35	116	0.0116	70.37

"	50	16.2	0.475	0.792	1	2.2	105	1.9	21.2	38	123	0.0123	70.24
Bkss	70	13.2	0.449	0.749	0.89	3.4	95	1.8	20.6	44	111	0.0111	65.66
"	90	12.3	0.43	0.717	0.91	1.6	90	1.8	18	45	107.5	0.01075	68.33
"	110	12.8	0.435	0.726	0.96	1.7	89	2.1	18.4	45	112	0.0112	66.84
"	130	12.1	0.427	0.712	0.93	2	111	2.1	19.2	59	109.5	0.01095	65.82
BCg	150	15.1	0.408	0.681	0.67	2.3	147	1.6	24	68	133	0.0133	73.12
Btkb	170	11.8	0.353	0.589	0.51	3.2	106	1.4	17.5	55	128.5	0.01285	80.52
"	190	10.8	0.37	0.617	0.59	2.5	116	1.4	17.5	71	117	0.0117	77.26
"	210	13.8	0.406	0.677	0.86	2.5	132	1.9	23.1	90	96.8	0.00968	68.58
"	230	11.6	0.423	0.706	0.73	2.3	120	1.8	18.4	90	108.5	0.01085	70.43
"	260	14.4	0.439	0.732	0.8	2.4	116	2	22.6	92	109.5	0.01095	69.62
Btk2b	280	10.4	0.431	0.719	0.91	2.4	136	2	17.4	88	106.5	0.01065	67.77
"	310	9.9	0.411	0.686	0.84	2.2	135	1.9	17.1	87	105.5	0.01055	69.09
Btk3b	340	8.2	0.429	0.716	0.84	2.2	134	2	16	91	111.5	0.01115	67.12
"	370	8.4	0.416	0.694	0.92	2.3	134	2.2	15.9	88	103.5	0.01035	66.18
"	400	9.5	0.437	0.729	0.86	2.3	129	1.9	17.3	88	108.5	0.01085	67.88
"	430	9.2	0.433	0.722	0.93	2.7	128	2	14.9	88	105	0.0105	68.63
R (limestone)	460	4.5	0.127	0.212	0.17	5.8	45	0.5	48.8	27	58.4	0.00584	61.11

Upper paleosol interval		Ag	Al	Al ₂ O ₃	As	Ba	Be	Bi	Ca	CaO	Cd	Ce	Co
Horizon	Depth (cm)	ppm	%	wt %	ppm	ppm	ppm	ppm	%	wt %	ppm	ppm	ppm
Bgss1	10	0.61	9.63	18.20	33.8	320	3.93	0.34	0.32	0.45	0.03	86.3	30.3
"	30	0.11	9.68	18.29	8.6	310	3.46	0.35	0.31	0.43	<0.02	65.7	12.1
Bgss2	50	0.12	9.39	17.74	4.8	320	3.25	0.34	0.2	0.28	0.02	108.5	24.9
Bgss3	70	0.12	9.36	17.69	3.9	330	3.73	0.4	0.25	0.35	0.03	73.6	28.9

"	90	0.11	9.21	17.40	3	330	3.68	0.34	0.23	0.32	<0.02	59.6	21.4
"	110	0.1	8.85	16.72	2.9	340	3.3	0.4	0.22	0.31	<0.02	85.7	20.4
"	130	0.1	7.43	14.04	2.4	280	2.34	0.22	0.17	0.24	<0.02	96.8	18.1
BCg	150	0.06	5.79	10.94	1.3	240	1.52	0.11	0.17	0.24	<0.02	66.7	12.2
Bssktb1	170	0.1	8.89	16.80	4.1	340	3.19	0.33	0.18	0.25	<0.02	46	15.1
"	190	0.08	8.36	15.80	4.5	300	2.97	0.33	0.17	0.24	<0.02	72.4	14.7
"	210	0.1	8.22	15.53	4.7	210	2.51	0.26	0.17	0.24	<0.02	36.4	11
Bsskt2b	230	0.08	9.1	17.19	4.8	140	2.45	0.25	0.25	0.35	<0.02	64	7.1
"	250	0.09	8.81	16.65	3.9	140	2.93	0.22	0.25	0.35	<0.02	98.4	8.8
"	270	0.06	8.6	16.25	6	140	2.68	0.22	0.24	0.34	<0.02	112.5	7.8
"	290	0.08	8.71	16.46	4	130	3.02	0.21	0.37	0.52	<0.02	83.4	6.2
Bsskb	310	0.06	7.62	14.40	3.6	120	2.45	0.18	4.38	6.13	0.03	39.9	5
"	330	<0.01	8.05	15.21	4.4	120	2.45	0.18	3.59	5.02	0.02	39.1	5.1
"	350	0.01	6.51	12.30	<5	120	1.67	0.14	11.15	15.60	0.05	51.5	6.6
R (limestone)	370	<0.01	3.08	5.82	<5	100	1.13	0.11	22.1	30.92	0.1	56.5	5.4

Upper paleosol interval		Cr	Cs	Cu	Fe	Fe2O3	Ga	Ge	Hf	In	K	K2O	La
Horizon	Depth (cm)	ppm	ppm	ppm	%	wt %	ppm	ppm	ppm	ppm	%	wt %	ppm
Bgss1	10	90	10.6	30.2	3.9	5.58	29.3	0.21	3.4	0.079	2.42	2.92	33.8
"	30	89	10.6	5.4	4.17	5.96	27.9	0.19	3.3	0.115	2.38	2.87	29.5
Bgss2	50	86	10.95	68.3	3.03	4.33	26.5	0.21	3.4	0.086	2.6	3.13	45.4
Bgss3	70	89	10.95	72.5	3.42	4.89	26.5	0.19	3.6	0.088	2.81	3.38	31.8
"	90	88	10.95	66.6	3.53	5.05	27.7	0.19	3.2	0.09	2.83	3.41	24.3
"	110	79	10.5	36.9	4.53	6.48	25.7	0.22	3.5	0.084	2.59	3.12	37.5

"	130	67	7.44	35.3	6.05	8.65	22.4	0.23	3.5	0.069	1.92	2.31	45.6
BCg	150	50	4.57	6.8	4.77	6.82	16.6	0.18	3.3	0.045	1.32	1.59	32.6
Bssktb1	170	85	10.35	15.7	4.7	6.72	28	0.19	3.3	0.088	2.65	3.19	19.2
"	190	76	8.95	29.9	5.44	7.78	26.1	0.23	3.2	0.076	2.25	2.71	33.4
"	210	91	9.97	20.6	4.82	6.89	24.3	0.19	3.3	0.078	1.93	2.32	15.5
Bsskt2b	230	103	13.55	32	5.74	8.21	24.2	0.23	3.5	0.078	1.8	2.17	24.5
"	250	97	14.4	27.1	4.32	6.18	24.7	0.21	3.1	0.083	2.02	2.43	39.6
"	270	94	14.8	31.4	5.07	7.25	24.6	0.24	3	0.078	2	2.41	49.8
"	290	98	14.9	22.7	4.73	6.76	23.9	0.2	3.1	0.07	1.93	2.32	31.4
Bsskb	310	86	12.5	18.1	4.21	6.02	21.8	0.17	2.7	0.071	1.83	2.20	18.2
"	330	88	14.15	15.3	4.2	6.00	21.6	0.05	2.9	0.065	1.96	2.36	19.5
"	350	60	9.51	15.1	5.17	7.39	17.45	0.08	2.1	0.074	1.68	2.02	24.3
R (limestone)	370	27	3.8	17	3.79	5.42	8.32	<0.05	0.9	0.061	0.75	0.90	24.7
Upper paleosol interval Horizon		Li	Mg	MgO	Mn	MnO	Mo	Na	Na2O	Nb	Ni	P	P2O5
	Depth (cm)	ppm	%	wt %	ppm	wt %	ppm	%	wt %	ppm	ppm	wt%	wt %
Bgss1	10	92.1	0.71	1.18	0.0177	0.0229	2.22	0.22	0.297	15.3	64.9	0.018	0.041
"	30	100.5	0.91	1.51	0.0505	0.0652	0.45	0.23	0.310	15.9	38.1	0.016	0.037
Bgss2	50	82.3	0.89	1.48	0.0096	0.0124	0.35	0.26	0.350	15.9	53.2	0.017	0.039
Bgss3	70	84.8	0.97	1.61	0.0106	0.0137	0.3	0.27	0.364	15.3	51.6	0.024	0.055
"	90	80.9	0.99	1.64	0.0095	0.0123	0.3	0.29	0.391	16.6	47	0.032	0.073
"	110	80.3	1.1	1.82	0.0127	0.0164	0.25	0.36	0.485	14.8	48.1	0.032	0.073
"	130	66.6	1.11	1.84	0.0121	0.0156	0.27	0.55	0.741	13.8	45.8	0.026	0.060
BCg	150	49.8	0.85	1.41	0.008	0.0103	0.25	0.64	0.863	10.4	32	0.02	0.046
Bssktb1	170	95.5	1.01	1.67	0.0089	0.0115	0.36	0.24	0.324	14.1	46.3	0.019	0.044

"	190	87.9	0.89	1.48	0.0096	0.0124	0.46	0.34	0.458	13.4	48.1	0.023	0.053
"	210	95	0.7	1.16	0.0064	0.0083	0.49	0.32	0.431	15.2	43.8	0.017	0.039
Bsskt2b	230	75.5	0.71	1.18	0.0054	0.0070	0.64	0.27	0.364	15.7	34.6	0.014	0.032
"	250	67.2	0.78	1.29	0.0055	0.0071	0.5	0.46	0.620	15.5	41.6	0.013	0.030
"	270	51	0.77	1.28	0.0058	0.0075	0.54	0.57	0.768	15.1	42.6	0.015	0.034
"	290	50.7	0.78	1.29	0.0053	0.0068	0.44	0.5	0.674	13.9	35.5	0.014	0.032
Bsskb	310	34.7	0.82	1.36	0.0178	0.0230	0.44	0.5	0.674	13.4	29.8	0.013	0.030
"	330	30.8	0.87	1.44	0.0154	0.0199	0.48	0.5	0.674	13.7	27.7	0.018	0.041
"	350	23.4	1.11	1.84	0.0461	0.0595	0.42	0.37	0.499	9.9	28.5	0.03	0.069
R (limestone)	370	14.4	2.04	3.38	0.128	0.1653	0.18	0.16	0.216	4.4	17.3	0.022	0.050

Upper paleosol interval		Pb	Rb	Re	S	Sb	Sc	Se	Sn	Sr	Ta	Te	Th
Horizon	Depth (cm)	ppm	ppm	ppm	%	ppm	ppm	ppm	ppm	ppm	ppm	ppm	ppm
Bgss1	10	40.9	175.5	0.003	2.14	1.22	18.7	2	3.7	155	1.12	0.05	12.7
"	30	12.1	160	<0.002	0.09	0.52	20	1	3.8	176	1.14	0.05	11.8
Bgss2	50	13.6	172	<0.002	0.12	0.52	18.3	1	3.7	158	1.22	0.07	13.9
Bgss3	70	12.7	154	0.002	0.1	0.51	18.7	1	3.7	161.5	1.26	0.07	12.5
"	90	8.8	156.5	<0.002	0.06	0.43	18	1	3.9	183.5	1.15	0.07	9.8
"	110	9.4	147	<0.002	0.05	0.43	18	1	3.5	170	1.21	0.07	13.1
"	130	6.8	119	<0.002	0.01	0.36	14.7	1	2.8	134	0.98	0.05	12.5
BCg	150	5.4	77.6	<0.002	0.01	0.25	10.4	1	1.9	94.6	0.82	<0.05	10.6
Bssktb1	170	10.8	117	<0.002	0.07	0.62	16.9	1	3.7	174	1.09	0.06	8.6
"	190	11.3	134	<0.002	0.01	0.69	17.6	1	3.1	203	0.96	0.05	11.3

"	210	10.4	97.8	<0.002	0.02	1	15.9	1	3.4	184.5	1.09	<0.05	8
Bsskt2b	230	8.2	136	<0.002	0.02	1.24	17.6	1	3.6	210	1.16	<0.05	12.4
"	250	6.3	152.5	<0.002	0.01	0.92	18	1	3.4	268	1.07	<0.05	11.8
"	270	6.7	162.5	<0.002	0.01	1.13	17.3	1	3.2	270	1.01	<0.05	12.3
"	290	6.4	140	<0.002	0.01	0.99	16.8	1	3.1	296	1.08	<0.05	11.6
Bsskb	310	6.3	116.5	<0.002	0.02	0.92	15.3	1	2.7	472	0.94	<0.05	9
"	330	7.2	172.5	<0.002	0.01	1.02	14.1	1	3	469	1.02	0.06	11.3
"	350	7.7	148.5	<0.002	0.02	1.03	13.7	1	2.2	907	0.73	0.07	7.9
R (limestone)	370	5.7	61	<0.002	0.01	0.28	10.3	1	1	1940	0.32	0.08	3.6

Upper paleosol interval		Ti	TiO2	Tl	U	V	W	Y	Zn	Zr	Zr	SiO2
Horizon	Depth (cm)	%	wt %	ppm	ppm	ppm	ppm	ppm	ppm	ppm	wt %	Wt%
Bgss1	10	0.454	0.757	0.87	14.9	138	1.8	17.7	61	120.5	0.01205	68.42
"	30	0.455	0.759	0.79	5	140	1.9	18.3	65	119	0.0119	69.67
Bgss2	50	0.468	0.781	0.83	3.4	129	2	29.1	74	113	0.0113	71.72
Bgss3	70	0.461	0.769	0.91	3.4	133	2	23.3	83	109.5	0.01095	70.77
"	90	0.455	0.759	0.81	2.6	132	1.8	25	85	117.5	0.01175	70.87
"	110	0.434	0.724	0.82	2.5	123	1.9	28.9	97	110.5	0.01105	70.19
"	130	0.391	0.652	0.56	2.2	101	1.5	31.6	109	118	0.0118	71.43
BCg	150	0.339	0.565	0.41	2.4	67	1.3	19.4	85	108	0.0108	77.50
Bssktb1	170	0.405	0.676	0.79	2.4	120	1.9	15.8	89	110	0.011	70.23
"	190	0.395	0.659	0.66	2.4	117	1.8	23.9	79	111	0.0111	70.80
"	210	0.433	0.722	0.67	2.5	119	2	15.9	55	114.5	0.01145	72.62
Bsskt2b	230	0.452	0.754	0.71	2.8	137	2	22.4	39	115.5	0.01155	69.72

"	250	0.438	0.731	0.7	2	112	1.7	21.8	45	113	0.0113	71.69
"	270	0.428	0.714	0.68	2	108	1.7	22.1	42	113	0.0113	70.93
"	290	0.432	0.721	0.73	2.1	111	1.7	16.2	38	103.5	0.01035	71.19
Bsskb	310	0.395	0.659	0.69	2.1	100	1.5	18.7	41	92.2	0.00922	68.48
"	330	0.391	0.652	0.81	2.1	107	1.7	18.9	42	103	0.0103	68.55
"	350	0.288	0.480	0.62	3.1	82	1.3	23.2	55	77.2	0.00772	59.71
R (limestone)	370	0.121	0.202	0.26	5	34	0.6	26.2	42	35.8	0.00358	52.91

APPENDIX B

Table B.1
Stable isotopic composition of pedogenic calcite

Sample ID	Sample location	Profile depth (cm)	mass(μ g)	Ampl 44	d13C/12C	STDEV	$\delta^{13}\text{C}$ (‰VPDB)	$\delta^{18}\text{O}$ (‰VPDB)
BU-145C1	UPI	145	179	3265	4.15	0.08	-6.65311533	-4.0236218
BU-145C2	UPI	145	263	4453	4.05	0.04	-6.76030461	-4.55151245
BU-255C1	UPI	255	240	3130	3.86	0.07	-6.94658598	-4.1011379
BU-255C2	UPI	255	244	2707	4.79	0.05	-6.01567908	-4.98956855
BU-265C1	UPI	265	250	3235	3.99	0.05	-6.81319932	-4.29993565
BU-265C2	LPI	265	250	1919	4.47	0.10	-6.34124652	-4.73318455
BL-40C1	LPI	40	266	4457	4.30	0.04	-6.50433021	-3.70684735
BL-40C2	LPI	40	279	5325	3.82	0.03	-6.98378226	-3.1439042
BL-40C3	LPI	40	331	2776	5.09	0.10	-5.72070858	-5.7191613
BL-40C4	LPI	40	255	4669	3.85	0.05	-6.96068457	-3.40900125
BL-40C5	LPI	40	224	4606	2.67	0.04	-8.13156747	-2.60679975
BL-75C1	LPI	75	245	3679	4.69	0.05	-6.12116853	-4.07700175
BL-75C2	LPI	75	358	5809	3.98	0.04	-6.82659798	-4.1037418
BL-75C3	LPI	75	314	6572	3.77	0.03	-7.03207743	-2.62182225
BL-135C1	LPI	135	341	3303	4.74	0.04	-6.06237441	-4.07279545
BL-135C2	LPI	135	211	2039	4.81	0.08	-5.9984808	-4.3575219
bu-340-1	UPI	340	278	5244	3.97	0.04	-6.8164172	-3.2722117
bu-340-2	UPI	340	381	7490	4.84	0.05	-5.9375780	-3.8052974
bu-340-3	UPI	340	264	5324	3.75	0.06	-7.0290235	-3.7608486
bu-340-4	UPI	340	201	844	9.08	0.19	-1.6998602	-8.4253739
bu-340-4	UPI	340	201	509	9.14	0.15	-1.6349278	-8.4242727

APPENDIX C

Table C.1
Stable isotopic composition of soil organic carbon

Sample location	Sample depth (cm)	Wt (mg)	Ampl44	d13C/12C	d13C/12C bc	$\delta^{13}\text{C}$	Ampl28	d15N/14N	$\delta^{15}\text{N}$	C wt %	N wt %
Lower paleosol interval	0	12.513	7334	-11.66	-11.54	-22.56	1074	1.21	0.80	0.28	0.13
Lower paleosol interval	10	11.852	7502	-11.62	-11.49	-22.52	1215	1.86	1.46	0.3	0.15
Lower paleosol interval	20	11.833	9840	-11.63	-11.53	-22.56	1443	2.02	1.61	0.39	0.18
Lower paleosol interval	30	9.295	7305	-11.85	-11.73	-22.76	1259	1.23	0.83	0.38	0.2
Lower paleosol interval	40	8.701	6349	-11.72	-11.57	-22.60	1260	1.58	1.18	0.35	0.21
Lower paleosol interval	50	11.694	7212	-11.65	-11.52	-22.55	1618	2.49	2.09	0.29	0.2
Lower paleosol interval	60	11.092	5679	-12.13	-11.98	-23.01	1470	1.40	0.99	0.25	0.19
Lower paleosol interval	80	9.19	6019	-11.86	-11.72	-22.74	1284	1.22	0.82	0.32	0.21
Lower paleosol interval	90	11.037	4986	-12.05	-11.88	-22.90	1403	1.63	1.23	0.22	0.18
Lower paleosol interval	100	10.636	4119	-12.01	-11.80	-22.83	1368	0.49	0.08	0.19	0.19
Lower paleosol interval	115	10.844	3968	-12.29	-12.09	-23.11	1392	1.46	1.06	0.18	0.19
Lower paleosol interval	130	10.473	3124	-12.03	-11.75	-22.77	1135	0.81	0.40	0.15	0.16
Upper paleosol interval	10	10.97	5302	-11.93	-11.76	-22.79	777	-0.70	-1.11	0.23	0.11
Upper paleosol interval	20	10.335	7100	-11.73	-11.60	-22.63	787	-0.61	-1.02	0.33	0.12
Upper paleosol interval	30	9.909	13965	-11.73	-11.67	-22.70	867	-0.03	-0.44	0.65	0.13
Upper paleosol interval	40	11.576	11980	-11.55	-11.48	-22.49	978	-0.02	-0.44	0.43	0.12
Upper paleosol interval	50	10.722	12993	-11.64	-11.57	-22.58	978	0.14	-0.29	0.5	0.13
Upper paleosol interval	60	9.327	16459	-11.29	-11.24	-22.24	943	-0.34	-0.77	0.75	0.15

Upper paleosol interval	70	9.747	10073	-11.80	-11.72	-22.73	1029	-1.21	-1.64	0.41	0.15
Upper paleosol interval	80	9.643	10571	-11.50	-11.42	-22.42	1063	0.09	-0.33	0.44	0.16
Upper paleosol interval	90	10.644	9913	-11.32	-11.23	-22.23	1198	1.85	1.43	0.37	0.16
Upper paleosol interval	100	10.067	9450	-11.60	-11.51	-22.51	1111	0.91	0.49	0.37	0.16
Upper paleosol interval	110	9.038	9475	-11.63	-11.54	-22.55	982	-0.23	-0.66	0.42	0.16
Upper paleosol interval	120	10.845	6528	-12.32	-12.21	-23.22	832	-1.87	-2.31	0.22	0.11
Upper paleosol interval	130	10.126	5136	-12.35	-12.22	-23.23	763	-2.12	-2.55	0.17	0.11
Upper paleosol interval	140	10.114	4547	-12.85	-12.72	-23.72	730	-1.05	-1.48	0.14	0.11
Upper paleosol interval	150	10.191	3589	-12.77	-12.60	-23.60	1153	0.51	0.08	0.1	0.17
Upper paleosol interval	160	11.202	4401	-12.44	-12.29	-23.30	896	-1.83	-2.27	0.12	0.12
Upper paleosol interval	170	11.154	5679	-12.30	-12.18	-23.19	947	-2.07	-2.50	0.18	0.12
Upper paleosol interval	190	11.831	12494	-11.69	-11.62	-22.63	1216	-0.52	-0.95	0.44	0.15
Upper paleosol interval	200	10.24	19206	-11.48	-11.43	-22.42	1307	0.26	-0.22	0.9	0.18
Upper paleosol interval	210	10.796	10322	-11.74	-11.67	-22.65	1252	-0.27	-0.75	0.49	0.16
Upper paleosol interval	220	9.977	6353	-12.20	-12.10	-23.08	1025	-0.06	-0.54	0.36	0.15
Upper paleosol interval	230	11.993	6235	-12.21	-12.10	-23.08	1322	1.68	1.21	0.29	0.16
Upper paleosol interval	240	10.507	6947	-11.94	-11.84	-22.82	1132	1.04	0.56	0.37	0.16
Upper paleosol interval	250	12.044	7500	-12.19	-12.10	-23.08	1359	3.02	2.56	0.35	0.16
Upper paleosol interval	260	11.472	6780	-12.06	-11.95	-22.93	1158	1.11	0.63	0.32	0.14
Upper paleosol interval	270	11.271	6882	-12.22	-12.12	-23.10	1150	1.23	0.75	0.33	0.14

Upper paleosol interval	280	11.236	7749	-11.96	-11.87	-22.85	1291	1.44	0.96	0.38	0.16
Upper paleosol interval	290	12.024	6371	-12.00	-11.88	-22.86	1429	0.51	0.03	0.29	0.17
Upper paleosol interval	300	12.067	5981	-12.00	-11.88	-22.86	1326	1.80	1.33	0.27	0.15
Upper paleosol interval	310	11.592	4886	-12.34	-12.21	-23.19	1384	1.43	0.96	0.25	0.17
Upper paleosol interval	320	11.725	4549	-12.24	-12.09	-23.07	1311	0.64	0.17	0.23	0.15
Upper paleosol interval	230	11.993	6235	-12.21	-12.10	-23.08	1322	1.68	1.21	0.29	0.16
Upper paleosol interval	240	10.507	6947	-11.94	-11.84	-22.82	1132	1.04	0.56	0.37	0.16
Upper paleosol interval	250	12.044	7500	-12.19	-12.10	-23.08	1359	3.02	2.56	0.35	0.16
Upper paleosol interval	260	11.472	6780	-12.06	-11.95	-22.93	1158	1.11	0.63	0.32	0.14
Upper paleosol interval	270	11.271	6882	-12.22	-12.12	-23.10	1150	1.23	0.75	0.33	0.14
Upper paleosol interval	280	11.236	7749	-11.96	-11.87	-22.85	1291	1.44	0.96	0.38	0.16
Upper paleosol interval	290	12.024	6371	-12.00	-11.88	-22.86	1429	0.51	0.03	0.29	0.17
Upper paleosol interval	300	12.067	5981	-12.00	-11.88	-22.86	1326	1.80	1.33	0.27	0.15
Upper paleosol interval	310	11.592	4886	-12.34	-12.21	-23.19	1384	1.43	0.96	0.25	0.17
Upper paleosol interval	320	11.725	4549	-12.24	-12.09	-23.07	1311	0.64	0.17	0.23	0.15

REFERENCES

- Berner, R.A., 2006, GEOCARBSULF: A combined model for Phanerozoic atmospheric O₂ and: *Geochimica et Cosmochimica Acta*, v. 70, no. 23, p. 5653–5664.
- Beerling, D.J., 2002, Low atmospheric CO₂ levels during the Permo-Carboniferous glaciation inferred from fossil lycopsids: *Proceedings of the National Academy of Sciences of the United States of America*, v. 99, no. 20, p. 12567–12571.
- Blakey, R.C., 2003, Carboniferous–Permian Palaeogeography of the Assembly of Pangea. In: Wong, Th.E. (Ed.), *Proceedings of the XVth International Congress on Carboniferous and Permian Stratigraphy*. Utrecht, 10–16 August 2003. Royal Netherlands Academy of Arts and Sciences, pp. 10-16.
- Blakey, R.C. Colorado Plateau Geosystems Inc., 2010, Global and Regional Paleogeography: <http://cpgeosystems.com/paleomaps.html> (accessed February, 2013).
- Brady, N.C., and Weil, R.R., 2002, *The Nature and Properties of Soils*, [Thirteenth edition]: New Jersey, Pearson Education, Inc., 960p.
- Breecker, D. O., Yoon, J., Michel, L.A., Dinka, T.M., Driese, S.G., Mintz, J.S., Nordt, L.C., Romanak, K.D., and Morgan, C.L.S., 2013, CO₂ concentrations in Vertisols: Seasonal variability and shrink-swell: In *New Frontiers in Paleopedology and Terrestrial Paleoclimatology* (S.G. Driese, and L.C. Nordt, eds.); SEPM Special Publication Volume 104, p. 35-46.
- Brewer, R., 1976, *Fabric and mineral analysis of soils*, [Second Edition]: New York, R.E. Krieger Publishing Company, 482 p.
- Brown, L. F., Jr., Iriarte, R. F. S., and Johns, D. A., 1990, Regional depositional systems tracts, paleogeography, and sequence stratigraphy, Upper Pennsylvanian and Lower Permian strata, north-central Texas: University of Texas at Austin, Bureau of Economic Geology Report of Investigations 197, 116 p.
- Cerling, T.E., 1991, Carbon dioxide in the atmosphere; evidence from Cenozoic and Mesozoic Paleosols: *American Journal of Science*, v. 291, no. 4, p. 377–400.
- Cerling, T.E., 1999, Stable carbon isotopes in palaeosol carbonates: *Special Publications of the International Association of Sedimentologists* No. 27, p. 43–60.
- Driese, S.G., and Ober, E.G., 2005, Paleopedologic and paleohydrologic records of precipitation seasonality from Early Pennsylvanian “underclay” paleosols, U.S.A.: *Journal of Sedimentary Research*, v. 75, p. 997 –1010.
- Driese, S. G., Ludvigson, G. A., Roberts, J. A., Fowle, D. A., González, L. A., Smith, J. J., and McKay, L. D., 2010, Micromorphology and stable-isotope geochemistry of historical pedogenic siderite formed in PAH-contaminated alluvial clay soils, Tennessee, USA: *Journal of Sedimentary Research*, 80, 943-954.
- Fitzpatrick, E.A., 1993, *Soil microscopy and micromorphology*: New York, John Wiley & Sons, 304 p.
- Gile, L. H., Peterson, F.F. and Grossman, R.B., 1966, Morphological and genetic sequences of carbonate accumulation in desert soils: *Soil Science*, v. 101, p. 347-360.
- Gastaldo, R.A., DiMichele, W.A., and Pfefferkorn, H.W., 1996, Out of the icehouse into the greenhouse: A Late Paleozoic analogue for modern global vegetational change: *GSA Today*, v. 6, no. 10, p. 2-7.

- Huang, Y., Bol, R., Harkness, D.D., Ineson, P., and Eglinton, G., 1996, Post-glacial variations in distributions, ^{13}C and ^{14}C contents of aliphatic hydrocarbons and bulk organic matter in three types of British acid upland soils: *Organic Geochemistry*, v. 24, p. 273–287.
- Krull, E.S., and Retallack, G.J., 2000, $\delta^{13}\text{C}$ depth profiles from paleosols across the Permian-Triassic boundary: Evidence for methane release: *Geological Society of America Bulletin*, v. 112, p. 1459–1472.
- Ludvigson, G.A., González, L.A., Metzger, R.A., Witzke, B.J., Brenner, R.L., Murillo, A.P., and White, T.S., 1998, Meteoric sphaerosiderite lines and their use for paleohydrology and paleoclimatology: *Geology*, v. 26, p. 1039–1042.
- Michel, L.A., Driese, S.G., Nordt, L.C., Breecker, D.O., Labotka, D.M., and Dworkin, S.I., 2013, Stable carbon isotope geochemistry of Vertisols formed on marine carbonates and implications for deep-time paleoenvironmental reconstructions: *Journal of Sedimentary Research*, v. 83, p. 300–308.
- Mintz, J.S., Driese, S.G., Breecker, D.O., and Ludvigson, G.A., 2011, Influence of changing hydrology on pedogenic calcite precipitation in Vertisols, Dance Bayou, Brazoria County, Texas, U.S.A.: Implications for estimating paleoatmospheric pCO_2 : *Journal of Sedimentary Research*, v. 81, p. 394–400.
- Montañez, I.P., Tabor, N.J., Niemeier, D., DiMichele, W.A., Frank, T.D., Fielding, C.R., Isbell, J.L., Birgenheier, L.P., and Rygel, M.C., 2007, CO_2 -forced climate and vegetation instability during Late Paleozoic deglaciation: *Science*, v. 315, p. 87–91.
- Montañez, I.P., 2013, Modern soil system constraints on reconstructing deep-time atmospheric CO_2 : *Geochimica et Cosmochimica Acta*, v. 101, p. 57–75.
- Moore, D.M., and Reynolds, R.C., 1997, X-ray diffraction and the identification and analysis of clay minerals, second edition: New York, Oxford University Press, 379 p.
- Mora, C.I., Driese, S.G., and Colarusso, L.A., 1996, Middle to Late Paleozoic atmospheric CO_2 from soil carbonate and organic matter: *Science*, v. 271, p. 1105–1107.
- Mora, C.I., Sheldon, B.T., Elliott, W.C., and Driese, S.G., 1998, An oxygen isotope study of illite and calcite in three Appalachian Paleozoic vertic paleosols: *Journal of Sedimentary Research*, v. 68, p. 456–464.
- Nordt, L. C., and Driese, S. D., 2010a, New weathering index improves paleorainfall estimates from Vertisols: *Geology*, v. 38, p. 407–410.
- Nordt, L.C., and Driese, S.G., 2010b, A modern soil characterization approach to reconstructing physical and chemical properties of paleo-Vertisols: *American Journal of Science*, v. 310, p. 37–64.
- Peyser, C.E., and Poulsen, C.J., 2008, Controls on Permo-Carboniferous precipitation over tropical Pangaea: A GCM sensitivity study: *Palaeogeography, Palaeoclimatology, Palaeoecology*, v. 268, p. 181–192.
- Raymond, A., and Metz, C., 2004, Ice and its consequences: Glaciation in the Late Ordovician, Late Devonian, Pennsylvanian-Permian, and Cenozoic compared: *The Journal of Geology*, v. 112, p. 655–670.
- Retallack, G.J., 1988, Field recognition of paleosols, in Reinhardt, J., and Sigleo, W.R., eds., *Paleosols and weathering through geologic time*: Geological Society of America, Special Paper 216, p. 1–20.
- Retallack, G.J., 2001, *Soils of the past: An introduction to paleopedology* [second edition]: Malden, Massachusetts, U.S.A., Blackwell Science, 404 p.

- Royer, D.L., Berner, R.A., and Beerling, D.J., 2001, Phanerozoic atmospheric CO₂ change: evaluating geochemical and paleobiological approaches: *Earth-Science Reviews*, v. 54, p. 349–392.
- Royer, D.L., 2006, CO₂-forced climate thresholds during the Phanerozoic: *Geochimica et Cosmochimica Acta*, v. 70, p. 5665–5675.
- Scotese, C.R. (2003) PALEOMAP, Earth History, Jurassic. [WWW document]. URL <http://www.scotese.com/jurassic.htm> (April 2003).
- Sheldon, N.D., Retallack, G.J., and Tanaka, S., 2002, Geochemical climofunctions from North American soils and application to paleosols across the Eocene–Oligocene boundary in Oregon: *Journal of Geology*, v. 110, p. 687–696.
- Tabor, N.J., and Montañez, I.P., 2002, Shifts in late Paleozoic atmospheric circulation over western equatorial Pangea: Insights from pedogenic mineral $\delta^{18}\text{O}$ compositions: *Geology*, v. 30, p. 1127–1130.
- Tabor, N.J., and Montañez, I.P., 2004, Morphology and distribution of fossil soils in the Permo-Pennsylvanian Wichita and Bowie Groups, north-central Texas, USA: implications for western equatorial Pangean palaeoclimate during icehouse–greenhouse transition: *Sedimentology*, v. 51, p. 851–884.
- Tabor, N.J., and Poulsen, C.J., 2008, Palaeoclimate across the Late Pennsylvanian–Early Permian tropical palaeolatitudes: A review of climate indicators, their distribution, and relation to palaeophysiographic climate factors: *Palaeogeography, Palaeoclimatology, Palaeoecology*, v. 268, p. 293–310.
- Veizer, J., Ala, D., Azmy, K., Bruckschen, P., Buhl, D., Bruhn, F., Carden, G.A.F., Diener, A., Ebner, S., Godderis, Y., Jasper, T., Korte, C., Pawellek, F., Podlaha, O.G., et al., 1999, $^{87}\text{Sr}/^{86}\text{Sr}$, $\delta^{13}\text{C}$ and $\delta^{18}\text{O}$ evolution of Phanerozoic seawater: *Chemical Geology*, v. 161, p. 59–88.
- Yancey, T. E., 1991, Controls on carbonate and siliciclastic sediment deposition on a mixed carbonate-siliciclastic shelf (Pennsylvanian Eastern shelf of north Texas), in Franseen, E. K., Watney, W. L., Kendall, C. G. St. C., and Ross, W., eds., *Sedimentary modeling: Computer simulations and methods for improved parameter definition*: Kansas Geological Survey Bulletin 233, p. 263–272.
- Yancey, T.E., Cleaves, A.W., 1990, Carbonate and siliciclastic sedimentation in late Pennsylvanian cycles, north-central Texas, *Field-Trip Guidebook #7*, Dallas Geological Society, p. 1-55.
- Yang, W., 1996, Cycle symmetry and its causes, Cisco Group (Virgilian and Wolfcampian), Texas: *Journal of Sedimentary Research*, v. 66, p. 1102–1121.
- Yang, W., Kominz, M.A., and Major, R.P., 1998, Distinguishing the roles of autogenic versus allogenic processes in cyclic sedimentation, Cisco Group (Virgilian and Wolfcampian), north-central Texas: *Geological Society of America Bulletin*, v. 110, p. 1333–1353.